

# POLITECNICO DI TORINO

Engineering Faculty

## MASTER THESIS IN MECHATRONIC ENGINEERING

*Development and Control of an Electro-Hydraulic Actuator for  
Off-Road Mobile Machines*



**Advisors:**

Prof. Luigi Mazza

Prof. Jacopo Sini

Prof. Andrea Vacca

**Candidate:**

Enrico Zanda

ACADEMIC YEAR 2020/2021



*A Chiara, che crede in me molto più di quanto non faccia io.*

*Ai miei nonni, mio orgoglio ed esempio.*

# **Acknowledgements**

I would like to thank: Professor Andrea Vacca, for the unique opportunity he gave me; Shaoyang Qu, who guided me on this long journey; Professors Jacopo Sini and Luigi Mazza for being always supportive, helpful, and understanding; all the other fantastic people in the lab, for being supportive and inspiring.

# Summary

## 1. Introduction

- 1.1 Electro-hydraulic actuators
- 1.2 Research goals
- 1.3 Outline

## 2. Fluid power: properties and applications

- 2.1 Fluid properties
- 2.2 Constitutive equations
- 2.3 Hydraulic actuation solutions

## 3. Model based approach and software

## 4. EHA on the test rig (experimental)

- 4.1 Valve flow mapping
- 4.2 Valve model development
- 4.3 PI velocity control
- 4.4 Considerations

## 5. EHA on the machine (simulation)

- 5.1 From the test rig to the real machine
- 5.2 Model linearization
- 5.3 Control development: Pressure Feedback
- 5.4 Semiactive ride control preliminary study
- 5.5 Considerations

## 6. Conclusions

## 7. Future work

## Bibliography

## Appendix: Bond Graph

# 1.Introduction

## 1.1 Electro-hydraulic actuators

An electro-hydraulic actuator (EHA) is an actuation system usually composed by a variable velocity electric motor connected to a fixed displacement hydraulic pump, that drives the motion of a hydraulic cylinder. The excellent torque-speed characteristic of electric motors makes them able to rapidly answer to load power demand on different operative conditions. They also include power regeneration capability, working as generators in case of assistive loads. When combined with hydraulic systems, characterized by high power density, the result is a powerful and compact actuation solution. For their advantageous characteristics, those systems are the first choice for the aerospace segment. Some application examples include thrust vectoring control [D2007], and fly-by-wire control of aircraft moving surfaces.

With the growing electrification trend in mobile machines, the EHA solution is gaining a lot of momentum in new unexplored sectors. Even in off-road machines segment the first electric/hybrid models, providing good expectations for this technology.

A new EHA\* architecture especially designed for off-road construction machines, was developed in the MAHA fluid power research center at Purdue University (figure 1.1)

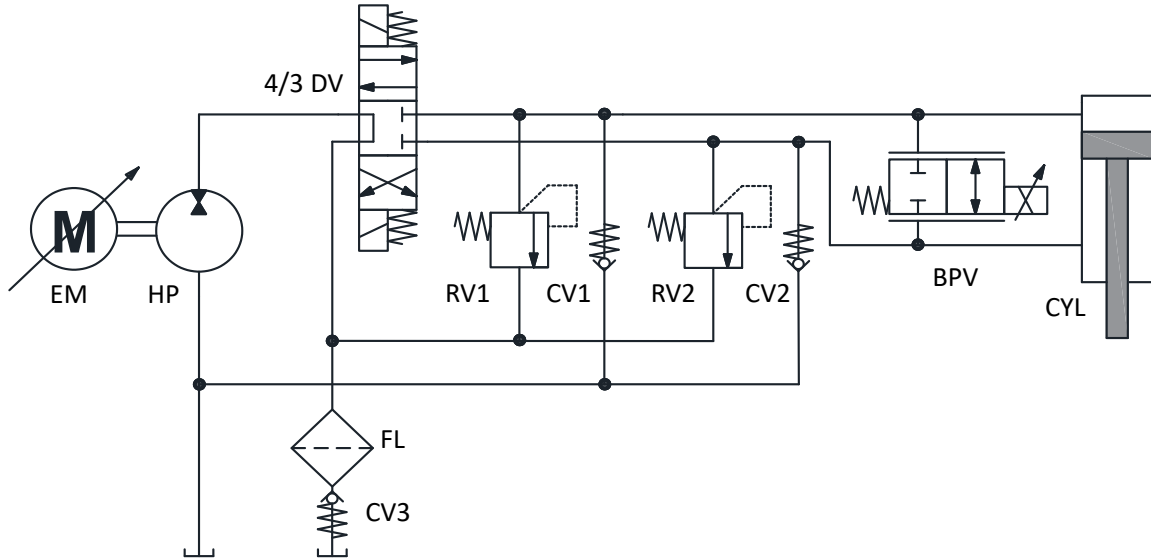


Figure 1.1: new EHA open circuit architecture for off-road applications. [Q2020]

It presents an open circuit configuration, with a two quadrants pump (HP), that can act as pump or as motor, depending on load conditions. A directional valve (4/3 DV) is included to invert the flow path and the cylinder velocity direction consequently. The peculiarity of this system is the implementation of a bypass valve (BPV), its function is to allow the EHA to work at low speeds, that would be unreachable by the pump alone, because of its minimum speed constraint.

---

\*From now on, when referring to electro-hydraulic actuator or EHA the new architecture described above is intended.

## 1.2 Research goals

The proposal of this research is to analyze and improve the dynamic behavior of the new EHA when installed in the reference machine, a CASE TV380 skid-steer (figure 1.2).

The EHA is going to replace the cylinders used to move the boom.



*Figure 1.2:Reference machine, CASE TV380 [machine user manual]*

The tasks to be accomplished are:

- Analysis of the critical dynamic issues of the new system, using the original hydraulic circuit present in the machine as a reference.
- Acceptable velocity reference tracking, regardless the system state (pump driven or BPV driven) and applied load. Ensuring smooth switch between states.
- Improve the dynamic behavior, solve the lack of damping typical of this high efficiency system, using special control strategies applied on the bypass valve. Aiming on comfort and safety improvement.
- Analyze the robustness of the control solution under different operative conditions.

- Exploit the laboratory test rig to acquire experimental data and test the improvements (within the setup limits).

## **1.3 Outline**

In the second chapter a brief introduction of fluid power is presented: starting from the fluid properties and the most relevant equations a lumped parameter approach for hydraulic systems is defined. An overall description of the main hydraulic actuation solutions is presented, focusing on efficiency, maneuverability, and the relation between the two. Those solutions are then compared with the EHA objective of this work. The third chapter explains the role of system model in simulation and in software design and test, together with the used software description. The fourth chapter describes the work done on the test rig, focusing on the bypass valve characterization and control improvement. The acquired data were also used to improve the EHA model. The fifth chapter describes how the EHA was integrated with the reference machine mechanics in the simulation environment. This complete model was then linearized in different operating points and a feedback control strategy was implemented to improve comfort maneuverability and safety. This paper ends with considerations on the work, achieved goals and issues, together with hints for future improvements.

## **2. Fluid power: properties and applications**

Fluid power is the technology that involves the use of pressurized fluids to perform mechanical actuation. The peculiarity that makes this solution unique among the main competitors, such as mechanical drives and electrical drives is the high power density. The hydraulic fluid can be highly pressurized and adapts itself to any geometric shape. Even a small amount of fluid can be easily directed to the power user by pipes or flexible hoses and can be converted into mechanical power through compact and lightweight devices. Furthermore, the simple and robust design, the ability to work under extreme conditions, the capability of the fluid to be also a heat vector, simplifying and decentralizing cooling, made FP the best choice for special applications, from aircraft & aerospace to heavy machinery employed in earth-moving, construction, and agriculture. Using fluid as a power vector also has few drawbacks: its compressibility results in a lack of stiffness, unlike electromechanical drives rigid couplings; motion control often uses throttling valves, resulting in low efficiency and imprecise reference tracking due to non-linearities and pressure dependency. The following paragraphs will examine the main fluid properties and the hydraulic systems constitutive equations, In the last part different hydraulic actuation solutions will be presented and compared.

## 2.1 Fluid properties

Hydraulic fluid is the medium by which the power is transmitted. Unlike mechanical transmission, where gears and shafts remain mainly unchanged through various operative conditions, the hydraulic fluid constantly changes its properties. Gibbs' phase law defines the number of variables sufficient to describe a fluid (equation 2.1).

$$f = n - k + 2 \quad (2.1)$$

Where  $f$  is the number of variables,  $n$  the number of components mixed inside the fluid, and  $k$  the number of present phases. Usually, the number of components can be assumed 1, as the number of phases. That is a reasonable assumption in nominal operative conditions but varies if turning away from them. Among the different variables that can be used, pressure and temperature are the most convenient to choose they are usually easy to measure and intuitive to use. [V2021]

### Bulk modulus

The volume that fluid occupies is not constant, and it can be parametrized using pressure and temperature. This relation can be expressed as a simplified linear function (equation 2.2) [V2021].

$$V = V_0 \cdot \left[ 1 - \frac{(p - p_0)}{B} + \gamma \cdot (T - T_0) \right] \quad (2.2)$$

Considering

$$B = -V_0 \left( \frac{\partial p}{\partial V} \right) \Big|_{T_0} \quad (2.3)$$

$$\gamma = -\frac{1}{V_0} \left( \frac{\partial V}{\partial T} \right) \Big|_{p_0} \quad (2.4)$$

Where **B** is called **Isothermal Bulk Modulus** and represents the volume variation with respect to pressure variation. And  $\gamma$  is **the volumetric expansion** coefficient that expresses the volume variation with temperature.

The bulk modulus is pressure dependent, as shown in figure [2.1], it is considered constant only after a certain pressure threshold. This threshold depends on the gas volume entrained in the liquid, quantified in the graph as  $r_v$ , the ratio between gas and liquid volume at atmospheric pressure.

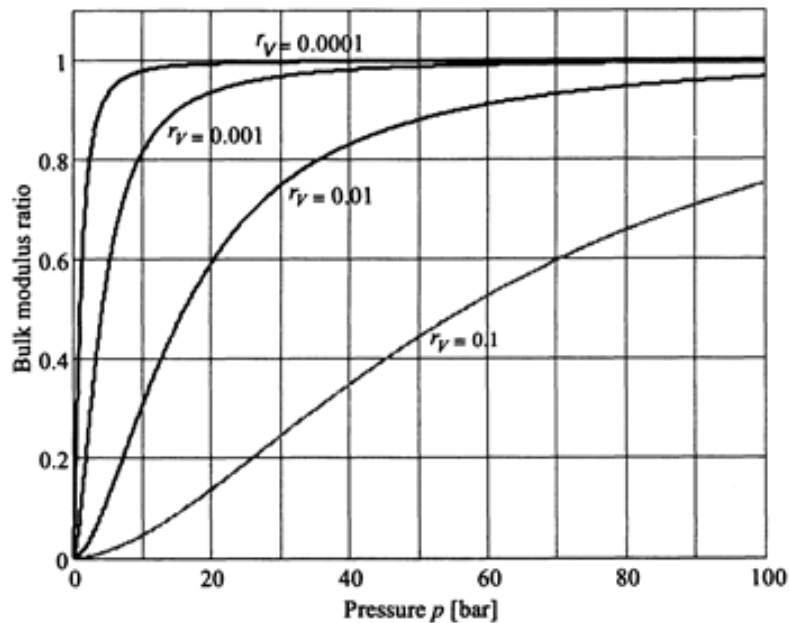


Figure 2.1: Bulk modulus pressure dependency considering gas and liquid volume ratio [J2003]

## Density

The fluid **density**  $\rho_0$  is the ratio between mass and volume, and it is usually defined at 1 Bar and 25 °C (equation 2.5).

$$\rho_0 = \frac{m_0}{V_0} \quad (2.5)$$

Differentiating equation 2.5 and considering  $\partial m = 0$  the **density-volume relationship** is obtained:

$$\rho \cdot \partial V + V \cdot \partial \rho = \partial m = 0 \quad (2.6)$$

## Viscosity

The viscosity is the measure of the fluid resistance against shearing force. The **dynamic or absolute viscosity  $\mu$**  is determined by the Newtonian shear stress equation (2.7). The relevant parameters are shown in figure [2.2].

$$\mu = \frac{\tau}{dv/dy} \quad (2.7)$$

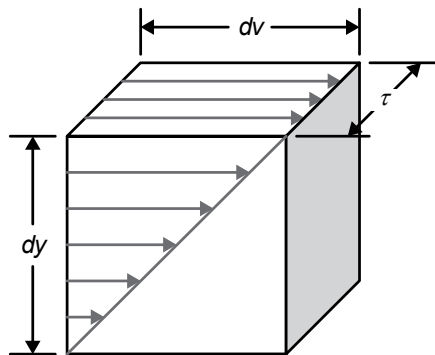


Figure 2.2: viscosity equation main parameters graphical representation

Where  $dv$  is the relative velocity between two surfaces,  $dy$  is the distance between them, and  $\tau$  is the shear stress.

Besides the ISO classification, the fluid properties can vary from brand to brand, as the method used to retrieve them. An accurate description is not fundamental when focusing on control design, but the influence of different oils and different operative conditions

ensures model robustness, and influences control consequently. Table [2.1] shows few oil properties examples, taken from the simulation software Simcenter Amesim.

Fluid	$\rho_0 \left[ \frac{kg}{m^3} \right]$	$B [bar]$	$\gamma \left[ \frac{1}{K} \right]$	$\mu [cP]$
Amesim Standard	860	17000	Not considered	51
ISO 32	868	16300	0.00066	37
ISO 46	872	16500	0.00066	55

Table 2.1: compared fluid properties.

## Flow regimes

Hydraulic fluid through pipelines and components can have two types of flow:

- 1) Laminar flow, when fluid follows smooth paths, divided into layers and without mix. There is no speed component in the direction perpendicular to the flow.
- 2) Turbulent flow, when a chaotic motion occurs and the fluid constantly mixes, creating vortices.

Velocity profiles (figure[2.3]) and fluid characteristics are different between the two.

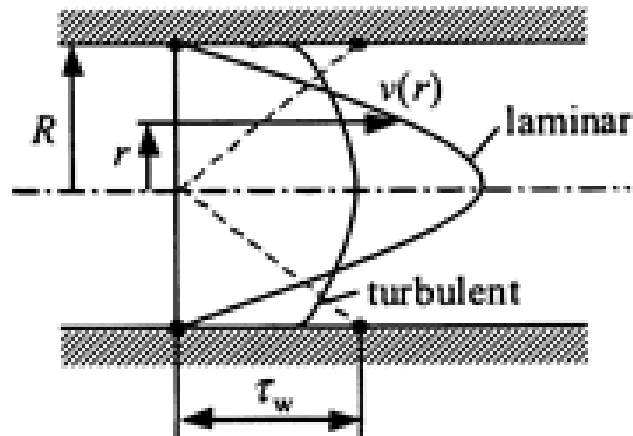


Figure 2.3: Flow velocity profiles in a pipeline [J2003]

The parameter that sets the bound between those regimes is called the Reynolds number (equation 2.8).

$$Re = \frac{\rho \cdot v_{avg} \cdot D_h}{\mu} \quad (2.8)$$

Where  $v_{avg}$  is the average stream velocity and  $D_h$  is the hydraulic diameter, correspondent to the geometric diameter when dealing with circular orifices. For common pipes  $Re < 2300$  corresponds to laminar flow, while  $Re > 4000$  corresponds to turbulent flow.

## 2.2 Constitutive equations

### Conservation of mass

An important principle that drives fluid mechanics is the **conservation of mass**. It states that the change rate of mass in a control volume is equal to the flux of mass across the control surface. (equation 2.9, figure [2.4]).

$$\frac{\partial}{\partial t} \cdot \int_{CV} \rho \cdot dV + \int_{CS} \rho \cdot \vec{u} \cdot d\vec{A} = 0 \quad (2.9)$$

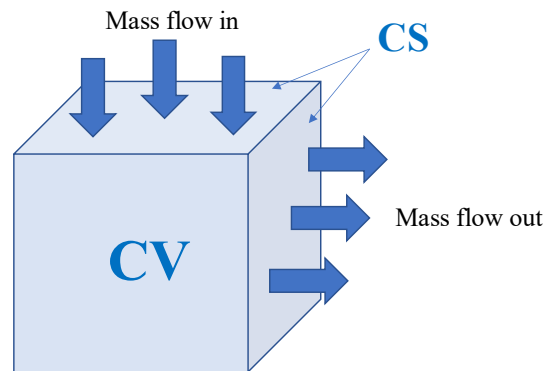


Figure 2.4: graphical representation of the conservation of mass control volume

Assuming incompressible fluid, a rigid volume, and uniform flow in each control surface port, a simple flow conservation law can be written.

$$\sum_{i=1}^N Q_i = 0 \quad (2.10)$$

That law will be later used to explain flow through multiport connections and cylinders.

## Fluid momentum

Newton's second law states that the forces acting on a system are equal to the time-rate-of-change of the system's momentum. In mechanical systems, this is described by the well-known  $F = \partial(m \cdot v)/\partial t = m \cdot a$ . In fluid mechanics, the same law is expressed as the **fluid momentum equation** (2.11).

$$F = \frac{\partial}{\partial t} \cdot \int_{CV} \rho \cdot \vec{u} \cdot dV + \int_{CS} \rho \cdot \vec{u} \cdot (\vec{u} \cdot d\vec{A}) \quad (2.11)$$

That equation is important to determine the flow forces acting on hydraulic components and will be especially used to determine the effect of flow force on valve spools.

Both conservation of fluid mass and momentum are applications of the **Reynolds Transport Theorem**, which rules the fluid properties inside a control volume. (a more detailed study can be found in F2020).

## Hydraulic resistance

The **hydraulic resistance** is the ratio between the differential pressure across a hydraulic component and the flow rate through it. The element that generates this resistance is usually an orifice, a sudden flow path restriction.

To represent this resistance, in turbulent flow regime, the **orifice equation** (2.12) is used. Where  $A$  is the passage area [m<sup>2</sup>],  $\rho$  is the fluid density [kg/m<sup>3</sup>],  $C_d$  is the coefficient of discharge.  $C_d$  usually goes from 0.6 to 0.8, based on the orifice geometry and it is usually experimentally determined and assumed constant. The following results in a nonlinear correlation between pressure and flow, but it can be linearized for small intervals (equation 2.13). That procedure is graphically described in figure [2.5].

$$Q = C_d \cdot A \cdot \sqrt{\frac{2 \cdot \Delta p}{\rho}} \quad (2.12)$$

$$R_{lin} = \frac{d(\Delta p)}{dQ} = 2 \cdot \sqrt{R_{turb} \cdot \Delta p} \quad (2.13)$$

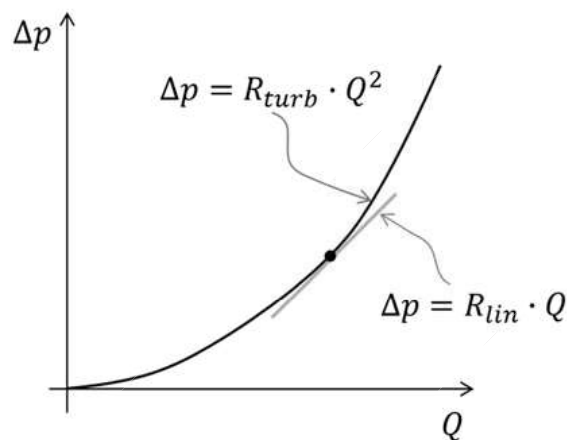


Figure 2.5: graphical representation of linearized hydraulic resistance [V2021]

The behavior of the fluid crossing an orifice is different in laminar conditions, a new correlation is then needed: Jelali (J2003) reports a linear correlation between flow and pressure (equation 2.14), which was theoretically determined by Wuest (W1954). It is valid for sharp circular orifices.

$$Q = \frac{\pi \cdot d^3}{50.4 \cdot \mu} \cdot \Delta p \quad (2.14)$$

Jelali also presents a study carried out by Viersma (Vi1980), where the orifice equation is extended to the laminar case by introducing a discharge coefficient as a function of Reynolds number (equation 2.15) introducing the laminar flow coefficient  $\delta$  (equation 2.16).

$$C_d = \delta \cdot \sqrt{Re} \quad (2.15)$$

$$\delta = \frac{C_{d,turb}}{\sqrt{Re_{crit}}} \approx 0.1366 \text{ (for sharp edges)} \quad (2.16)$$

The discharge coefficient, function of  $\sqrt{Re}$  is shown in figure [2.6]. After the critical Reynolds number  $C_d$  reaches its turbulent value and stays constant.

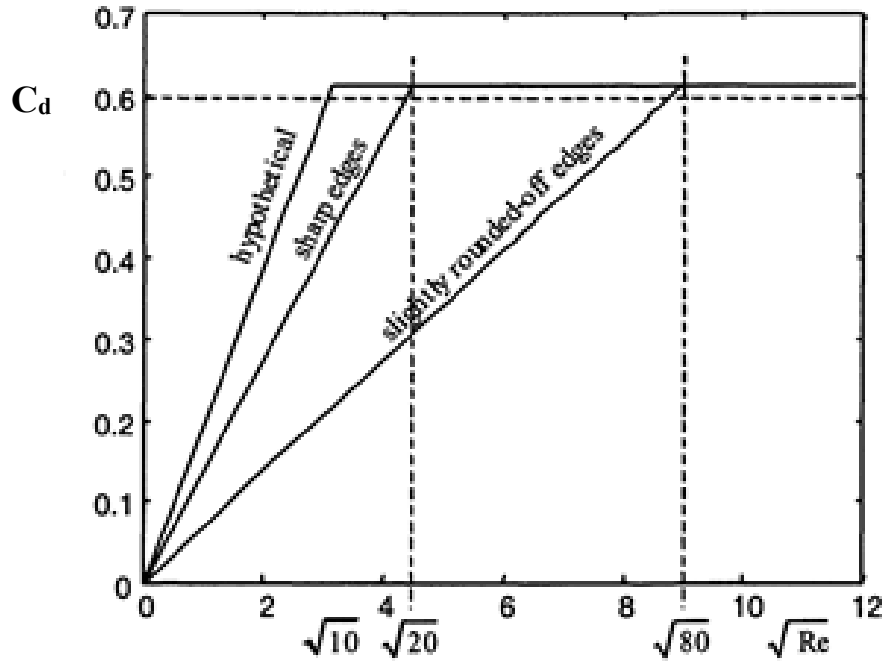


Figure 2.6: Discharge coefficient correlation with  $Re$  [J2003]

The solution that was adopted by Simcenter Amesim, the simulation software used in this study, follows a similar logic (S2019). A parameter  $\lambda$ , called **flow number** is used (equation 2.17).

$$\lambda = \frac{d}{\nu} \cdot \sqrt{\frac{2 \cdot |\Delta p|}{\rho}} \approx Re_h \quad (2.17)$$

It is similar to the differential pressure-based Reynolds number formulation by Lichtarowicz (L1965) and also reported by Jelali (J2003) as  $Re_h$ . A  $\lambda_{crit}$  can then be used as a threshold between laminar and turbulent regimes.

In Amesim the discharge coefficient is then expressed as a function of lambda, following equation (2.18). That function converges to  $C_{d,turb}$  when  $\lambda_{crit}$  is reached (figure [2.7]). Using this  $C_d$  the classical orifice equation, both flow regimes are covered. A similarity

can be found between figures[2.6] and [2.7]. According to the Amesim user manual,  $\lambda_{crit}$  lays between 50000 for really smooth geometries and 50 for complex shapes; the default value is set to 1000.

$$C_d = C_{d,turb} \cdot \tanh\left(\frac{2 \cdot \lambda}{\lambda_{crit}}\right) \quad (2.18)$$

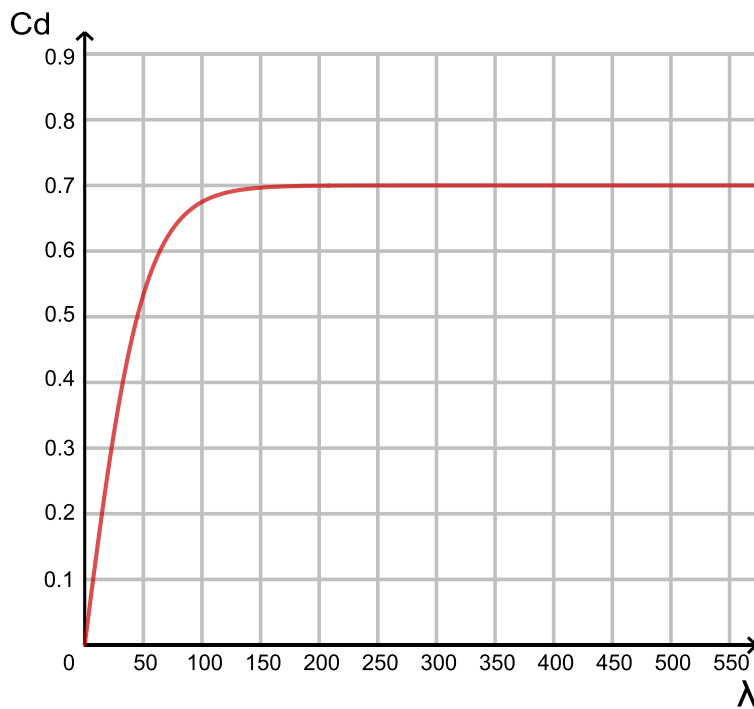


Figure 2.7: Discharge coefficient correlation with flow number in Amesim

## Hydraulic capacitance and pressure build-up equation

The first term of conservation of mass equation (2.9) can be simplified considering uniform fluid density ( $\rho$  out of the integral) and expressed as follows:

$$\frac{\partial}{\partial t} \cdot \int_{CV} \rho \cdot dV = \frac{\partial}{\partial t} (\rho \cdot V) = \rho \cdot \frac{\partial V}{\partial t} + V \cdot \frac{\partial \rho}{\partial t} \quad (2.19)$$

The second term of (2.9) can be simplified by considering uniform flow:

$$\int_{CS} \rho \cdot \vec{u} \cdot d\vec{A} = \sum \rho \cdot Q_{out} - \sum \rho \cdot Q_{in} \quad (2.20)$$

Combining 2.19 and 2.20:

$$\frac{V}{\rho} \cdot \frac{\partial \rho}{\partial t} = \sum Q_{in} - \sum Q_{out} - \frac{\partial V}{\partial t} \quad (2.21)$$

Density in isothermal conditions can be reduced as only pressure dependent, so that:

$$\frac{\partial \rho}{\partial t} = \left. \frac{\partial \rho}{\partial p} \right|_T \cdot \frac{\partial p}{\partial t} \quad (2.22)$$

Including bulk modulus (2.9) and considering density-volume correlation (2.6):

$$\frac{\partial \rho}{\partial t} = \frac{\rho}{B} \cdot \frac{\partial p}{\partial t} \quad (2.23)$$

Substituting 2.23 into 2.21 the result is the so-called **pressure build-up equation 2.24**, which describes pressure transients in hydraulic components. Note that the volume variation term can be neglected in the case of rigid control volumes.

$$\frac{\partial p}{\partial t} = \frac{B}{V} \left( \sum Q_{in} - \sum Q_{out} - \frac{\partial V}{\partial t} \right) \quad (2.24)$$

Using the pressure build-up equation, a **hydraulic capacitance** is defined as follows:

$$C_H = B/V \quad (2.25)$$

Such that:

$$p(t) = \frac{1}{C_H} \cdot \int \sum Q(t) \quad (2.26)$$

## Hydraulic inertia

Applying fluid momentum equation (2.11) to a rigid pipe section (figure[2.8]) some simplifications can be made: the last term can be neglected considering inlet and outlet flow properties approximately unchanged; the system can be considered as unidimensional (all the vectors have x component only); the external force F acting on the control volume correspond to the pressure differential multiplied by the section area; the rate of change of momentum can be written as follows:

$$\frac{\partial}{\partial t} \cdot \int_{cv} \rho \cdot \vec{u} \cdot dV = m \cdot \frac{\partial u_x}{\partial t} = \rho \cdot L \cdot A \cdot \frac{\partial u_x}{\partial t} \quad (2.27)$$

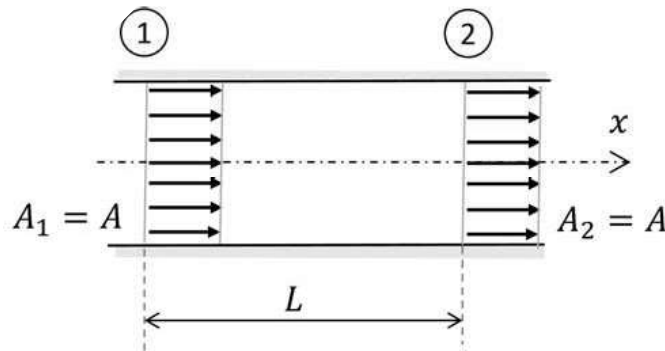


Figure 2.8: Flow through a pipe with constant velocity profile [V2021].

Those assumptions lead to the following equation:

$$(p_1 - p_2) = \frac{\rho \cdot L}{A} \cdot \frac{\partial Q}{\partial t} = L_H \cdot \frac{\partial Q}{\partial t} \quad (2.28)$$

Where  $L_H$  is the hydraulic inductance.

## Lumped parameter approach

The hydraulic resistance, capacitance, and inductance previously developed are the fundamental blocks used to build hydraulic dynamic models. Those can be associated with other equivalent blocks in different domains. Figure [2.9] shows the correlation between hydraulic and electric components.

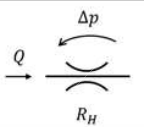
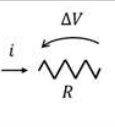
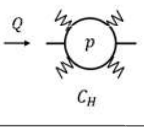
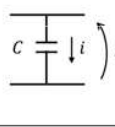
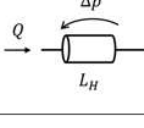
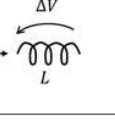
ELEMENT	SYMBOLIC REPRESENTATION	FORMULA	ELECTRIC ANALOG	SYMBOLIC REPRESENTATION	FORMULA
HYDRAULIC RESISTANCE		$\Delta p_{LAM} = R_{LAM} Q$ $\Delta p_{TUR} = R_{TUR} Q^2$	ELECTRIC RESISTANCE		$\Delta V = Ri$
HYDRAULIC CAPACITANCE		$\frac{dp}{dt} = \frac{1}{C_H} Q$	ELECTRIC CAPACITANCE		$\Delta V = \frac{1}{C} \int i dt$
HYDRAULIC INDUCTANCE		$\Delta p = L_H \frac{dQ}{dt}$	ELECTRIC INDUCTANCE		$\Delta V = L \frac{di}{dt}$

Figure 2.9: Lumped parameter approach: hydraulic and electric analogy [V2021].

These simplified discretized elements can be used to describe a physical model through differential equations. That is called **lumped parameter approach**. Software like Simcenter Amesim use it to model a wide range of mechatronic systems. It will also be used to develop linear models of the system in the following chapters.

## 2.3 Hydraulic actuation solutions

Many hydraulic power transmission variants were developed, each of them aimed to find the best balance for performance, efficiency, and costs. Some of them are presented in the following paragraph. The study of their different characteristics was the starting point to understand dynamic performance requirements and the role of the main components involved. Some of the schematics present on this paragraph are highly simplified, to give a rapid understanding of the circuits without needing a deep knowledge on fluid power systems.

### Traditional valve-controlled systems

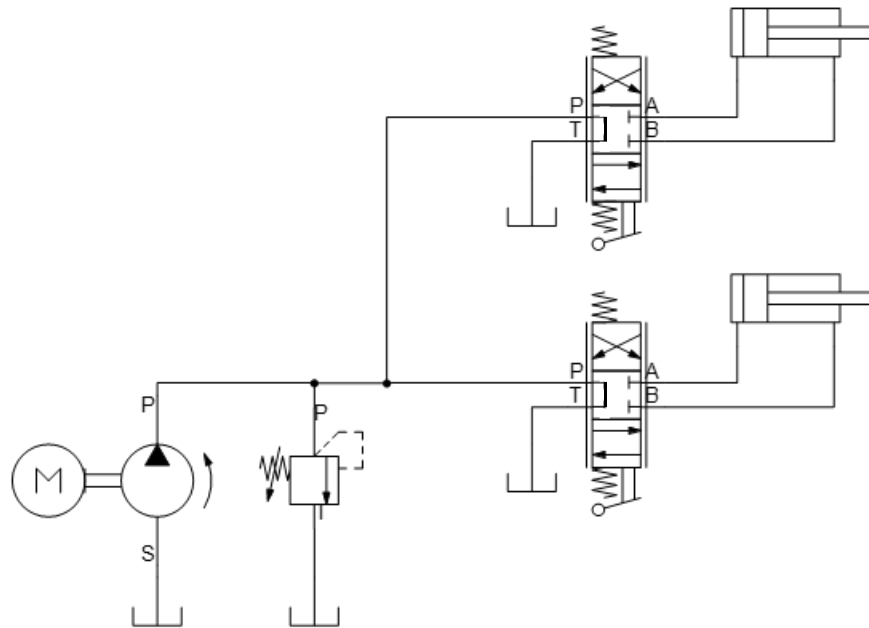


Figure 2.10: simplified schematic of a traditional valve driven velocity control with multi users

The traditional solution [2.10], common among mobile machines, presents a system based on a fixed displacement pump connected to a Diesel motor.

The pump always provides the same flow rate, the load defines the operative pressure, while the relief valve ensures a pressure limit in the line that serves all the valves. These valves act as variable resistance that controls the pressurized fluid going to the user. In some operative conditions, the user may not require all the flow that the pump provides. In this case, just a part of the generated power is sent to the user, the other part is wasted through the pressure relief valve. This system has the worst efficiency performance but relies on a low-cost simple configuration. From the dynamic behavior point of view, the throttling created by the control valve in both the cylinder chambers results in a smooth and relatively well-damped motion, at the cost of an increased power loss.

Some upgrades can reduce the power waste, increasing the complexity and therefore the cost of the system. Using variable displacement pumps the flow delivered can be adapted to the user speed requirements, that's called flow-sensing control. This technique saves the energy wasted due to flow excess but is not able to act on pressure excess. The more advanced solution, able to solve that last issue is the load-sensing control, also called power-matching control. The main differences between these techniques are explained in the following pictures [2.11]. The corner power is the maximum deliverable pump power. Pump design and shaft speed limit the maximum flow rate, while a relief valve limits the pressure, protecting the hydraulic components. The metering point power is the power that the user (e.g. a cylinder) needs to receive at the desired speed, considering its load.

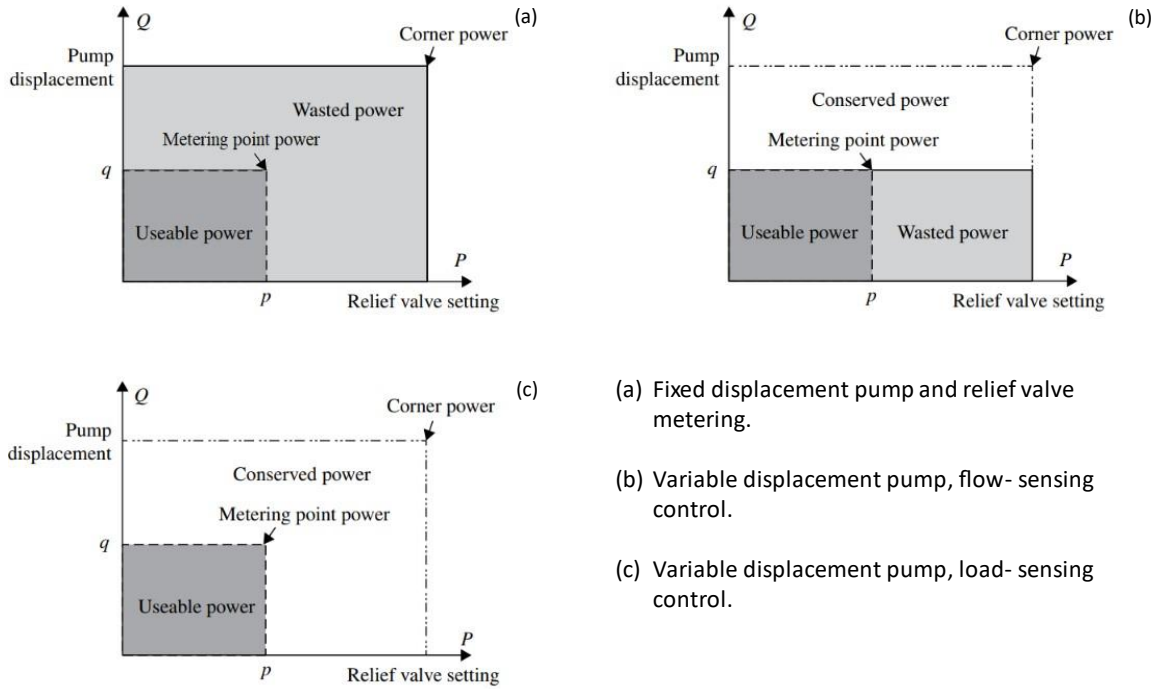


Figure 2.11: power consumption for different pump control strategies [Z2018]

## Independent metering

The traditional systems are the worst-case scenario in terms of efficiency: being the power unit centralized and far from the implement, long pipes and hoses are needed, moreover the common directional valves, used to control the cylinders, throttle both cylinder inlet and outlet when performing metering, because of the mechanical coupling between ports.

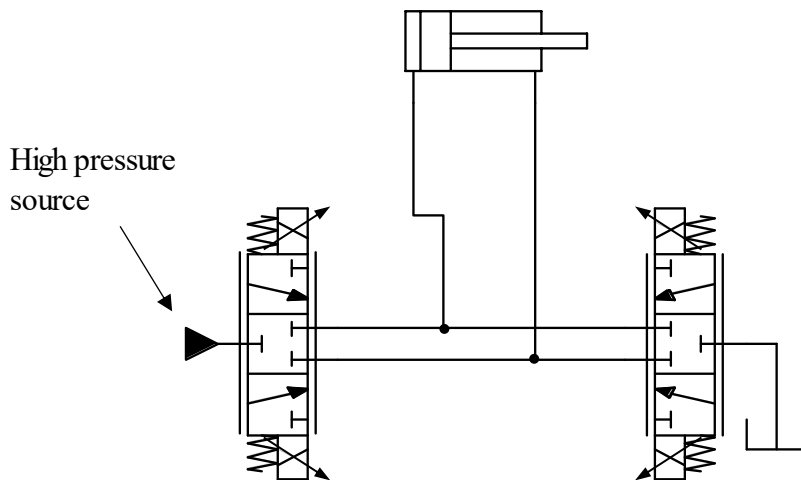
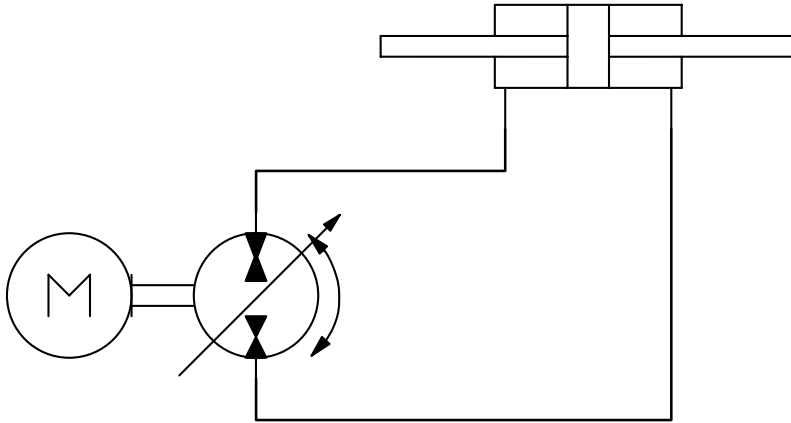


Figure 2.12: independent metering simplified, this solution limits outlet throttling improving efficiency.

To limit a part of those throttle loss, a further step was done by introducing an independent metering technique []. It consists of decoupling cylinder inlet and outlet flow control, using a valve for each port. In that way, it is possible to free the path from the cylinder outlet chamber to the tank by keeping its relative valve wide open and, doing so, reducing part of the throttle loss. Meanwhile, the valve connected to the inlet modulates the cylinder speed. The main independent metering drawbacks are increased overall costs and complexity, and a lack of damping.

The independent metering moreover adds flexibility to the control strategy, in [D2017] the valve connected to the inlet drives the velocity while the outlet valve is used to damp the oscillations by using a pressure feedback control.

## Displacement control



*Figure 2.13 Simplified displacement control architecture, the cylinder is directly driven by the pump, with the lowest possible throttling loss*

Displacement controlled systems (figure [2.12]) use a totally different approach, they are pump driven systems, meaning that each actuator has its own pump. By varying the pump displacement, the amount of sent flow is commanded, and converter into cylinder velocity. The pump is usually able to operate in all the 4 quadrants, allowing power regeneration in case of assistive loads. The main loss in this system is in the pump efficiency, it is usually high, tendentially lower at low speeds. It is the perfect solution for hydraulic machines with a limited number of users. This low throttling architecture has a drastically low damping, an electronic aid system is necessary to improve comfort and stability.

## **Considerations and comparisons with EHA**

From the analysis of those different solutions, some considerations can be made.

- The throttling is the key for both energy efficiency and maneuverability.
- High throttling systems can still be controlled by the operator directly acting on the valve pilot lines.
- With the increase of efficiency an electronic aid is usually chosen to help in reducing unwanted oscillations.

The EHA presents similar characteristics to the displacement controlled systems, a low damping is expected and therefore electronic solutions must be considered. But our system also includes a valve that drives the system at low speeds, that feature improves the reachable speed range compared to DC systems. The drawback of having pump driven states and valve driven states constantly switching in the same machine is that a common velocity reference must be followed to ensure a smooth switch. Those considerations will motivate the following chapters studies.

### 3. Design and testing procedure.

With the increasing complexity of modern mechatronic systems, multi-domain simulation gained great momentum. Fusing all the main domains in a single model allowed the development of an accurate prediction of the real product. The present EHA is an example of a specialized electro-hydraulic system, acting on a complex mechanical load and supervised by a structured control system.

Since reliable software is essential for good performance and safety, and the time to market has to be reduced as maximum as possible, MBSD (model based software design) alongside techniques to validate and test the developed software, it is needed before implementing the EHA in the real machine.

#### The V-model

A highly adopted development and validation approach is the V-model (figure [3.1]). It is a system development lifecycle used in different variants, depending on the application field. One of those, applied to the automotive field, is presented in the standard ISO 26262 "Road vehicles - Functional safety".

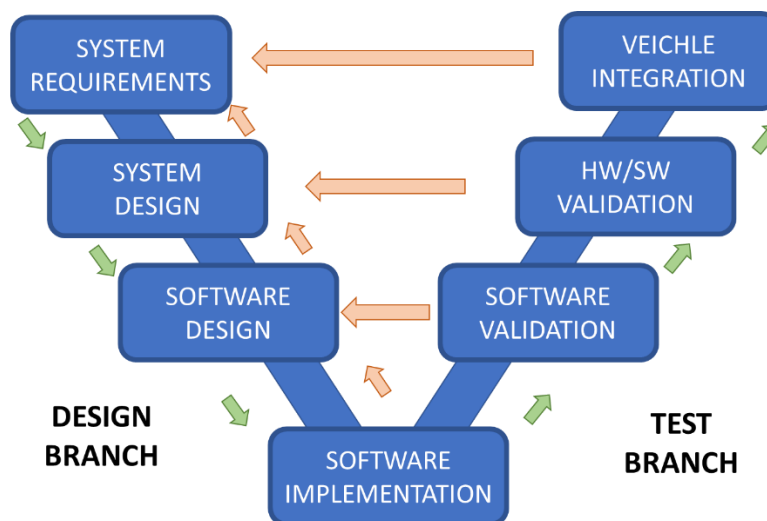


Figure 3.1: V-model applied to embedded software development.

The V-model guidelines are here briefly presented:

The starting point is a model of both plant and controller. Thanks to it, a model-in-the-loop test is performed, allowing iterative simulations to refine the model, finding potential issues and improvements on the design.

The controller model is then converted into code and tested alongside the plant simulation. That so-called software-in-the-loop test can check eventual errors in the code generation and give information about needed memory and computational power.

After that, The automatically generated code is deployed into target hardware, interfaced with the simulated plant. That procedure is called processor-in-the-loop and it is useful to test the code under the limited resources restrictions of embedded hardware.

Before reaching the real machine, a test to verify the correctness of the integration of the various software components is performed. It involves the embedded controller and the plant model implemented on real-time emulation hardware. That it is called hardware-in-the-loop and ensures the capability of the controller to act within real-time constraints.

The V-model must be considered as an iterative procedure. Each step on the design branch receives feedback from its following steps. The test branch adjusts and validates the entire chain. This process ensures early detection of faulty design choices, saving time and costs.

## **Software choice**

The previous chapter explained the importance of the model in the design and test process. In this section, the software environment choice is discussed. Siemens Simcenter Amesim, a multi-domain simulation software, was adopted for several studies relative to hydraulic systems. It was also used by MAHA researchers in the preliminary EHA, proving accurate results. But the remarkable characteristic, that made Amesim the definitive choice, is the capability to interface with Matlab and Simulink.

That expanded its usage, not only for standalone plant model development but also as plant-control logic integration, as shown in the following chapters.

The following sections will present the different concurrent simulation types used in this study.

### **SL2AMECosim: Simulink as slave, Amesim as master**

That solution allows creating an Amesim block from a Simulink system that will act as a slave.

A Matlab command will convert the Simulink file into an Amesim submodel by code generation. The solver and time steps used are the ones selected in Simulink before, Amesim will interact with the Simulink slave every time step by default (figure [3.2]). When using SL2AMECosim is not necessary to have Simulink running in the same machine.

That configuration is useful when custom Simulink code must control the plant while performing recursive simulations in the Amesim environment, such as batch run and optimization algorithm. In these cases, the control model stays the same while progressive

changes in the plant model are automatically applied; to show the influence of some design parameters in the overall behavior.

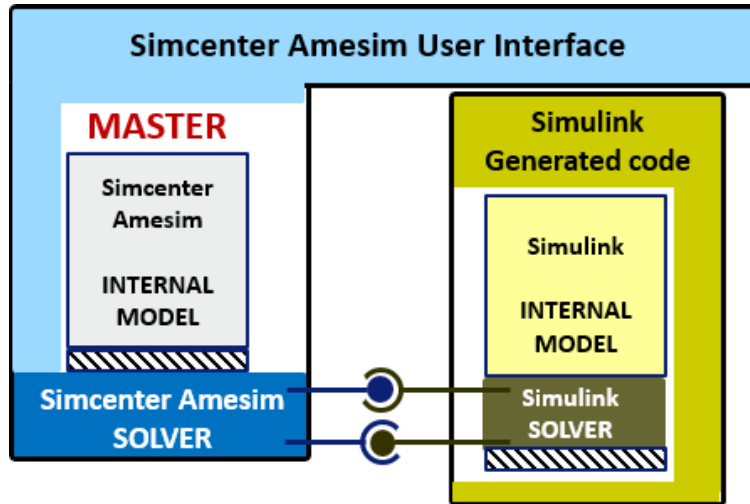


Figure 3.2: SL2AMECosim

## AME2SLCosim: Amesim as slave, Simulink as Master

This configuration requires both software running at the same time, Simulink starts the simulation, and a communication interface is used to share data between the two. In this case, the Amesim model is seen by Simulink as a discrete-time block.

During the simulation, and once it is complete, the user can access both the user interfaces, plotting data, look at 3D animation motion, and modifying control parameters. Even if it is not a real-time simulation, it is still possible to change inputs dynamically and observe the overall response.

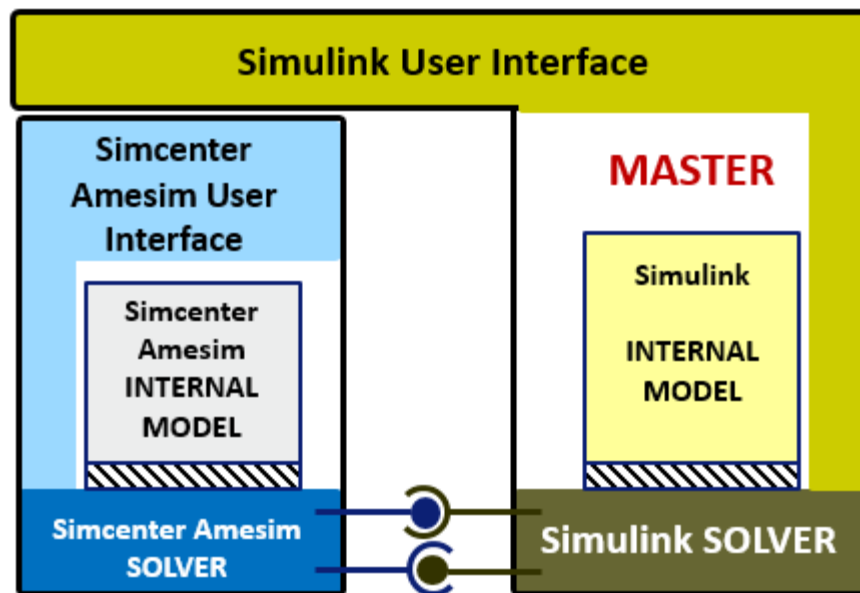


Figure 2.3: AME2SLCosim

## Test rig Model-in-the-Loop simulation

A virtual copy of the EHA physical system and its control logic was made to help in experimental data comparison and debugging. The virtual model must have the following characteristics:

1. The same control algorithm developed in Simulink for the test rig is needed: having the same filters, state logic, sampling time, experimental data comparison will be more reliable.
2. The control algorithm must be easily editable. Custom control data log is useful for debugging purposes and performance analysis. These are the reasons to prefer a simulation environment as Simulink to a static generated code.
3. The code must be modular and plug and play: any modification tested in the simulation can be copied in the real test rig control as it is.
4. The electro-hydraulic model must contain all the main non-linearities of the real counterpart.

Considering these requirements, we opted for the AME2SLCosim (figure [3.4]). This Model-In-the-Loop technique merges the main strengths of both software: Simulink extended control capability and Amesim advanced electro-hydraulic modeling. This simulation choice was proved as effective in literature, especially for hydraulic systems.

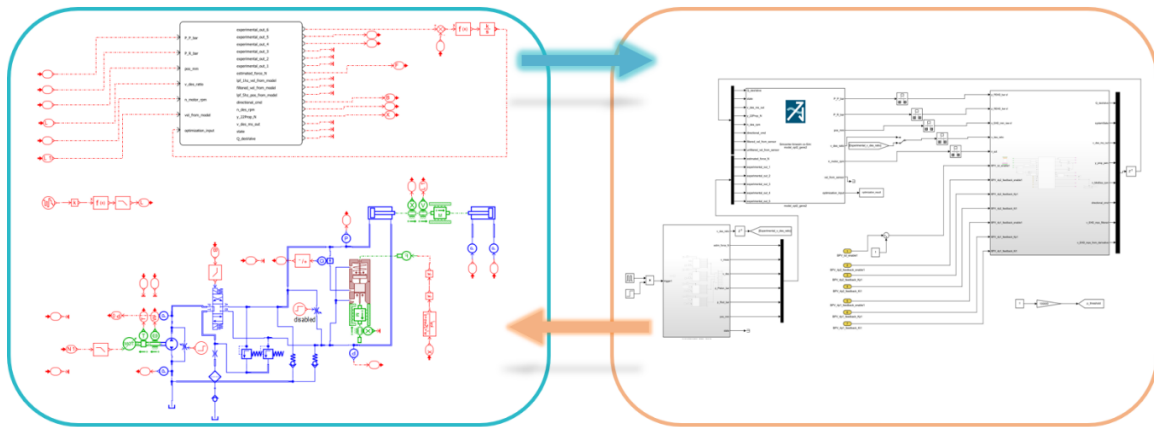


Figure 3.3: AME2SLCosim used to design the test rig control.

## 4. EHA on the test rig (experimental)

### 4.1 Valve flow mapping

Traditional systems use a single valve to drive the cylinder in the entire velocity range, the proposed EHA switches between two drivers: the velocity is driven by motor rpm variation in Pump-driven states, and by valve opening variation in bypass valve-driven states.

To give the operator perception of continuous variation, even while state switches occur, is important for both pump control and valve control to have a common velocity reference to track.

The pressure influence on the valve must be considered to make the velocity control load independent. Since the BPV used is not hydraulically pressure compensated, an electronic pressure compensation was implemented via experimental flow mapping. The flow mapping does not only consider pressure, but also the other non-linearities between input command value and desired flow through the valve.

Several experimental tests were made to generate the map. In Simulink, a state machine based on Stateflow was built to automatize the test. The valve input voltage (that spans from 0 to 10 V) was gradually increased with 1 V steps, 5 seconds long, until the maximum flow requirement was reached. All the procedure was repeated for different constant load forces. The working state used was low-speed assistive retraction (figure [4.1]) with motor speed set to 0 rpm. The flow through the BPV was back-calculated from cylinder velocity, which implies that the leakage through the pump, connected to the high-pressure line, must be considered. That leakage was assumed constant with pressure and calculated by applying constant force to the cylinder while keeping the BPV closed.

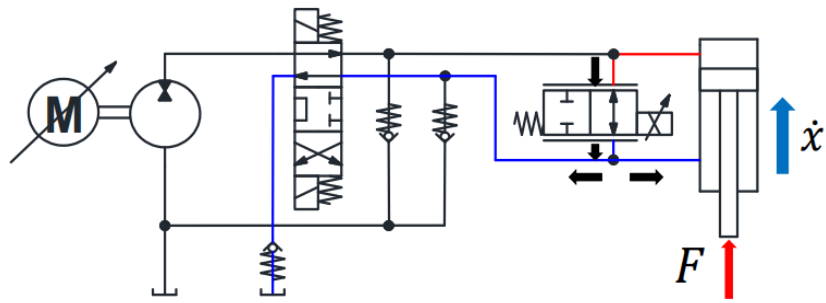


Figure 4.1: Assistive retraction state, used to extract the pressure-flow characteristic of the valve [Q2020]

The different datasets were post-processed in MATLAB and then converted into a lookup table. It accepts pressure difference between the valve ports and desired flow as inputs, returning as output the correspondent BPV voltage to apply [4.2].

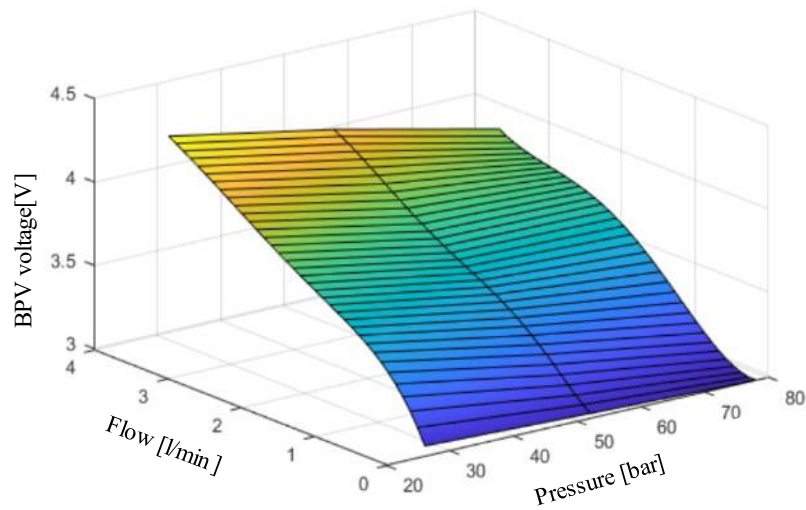


Figure 4.2: flow-pressure  $\rightarrow$  voltage map (lookup table)

Figure [4.3] shows a comparison between the original open-loop control and the improved flow mapping control. The test was made close to the switching between different drives (BPV only and pump only) and at constant pressure. The new control shows a good adaptation to the pressure and guarantees a constant slope regardless of the state.

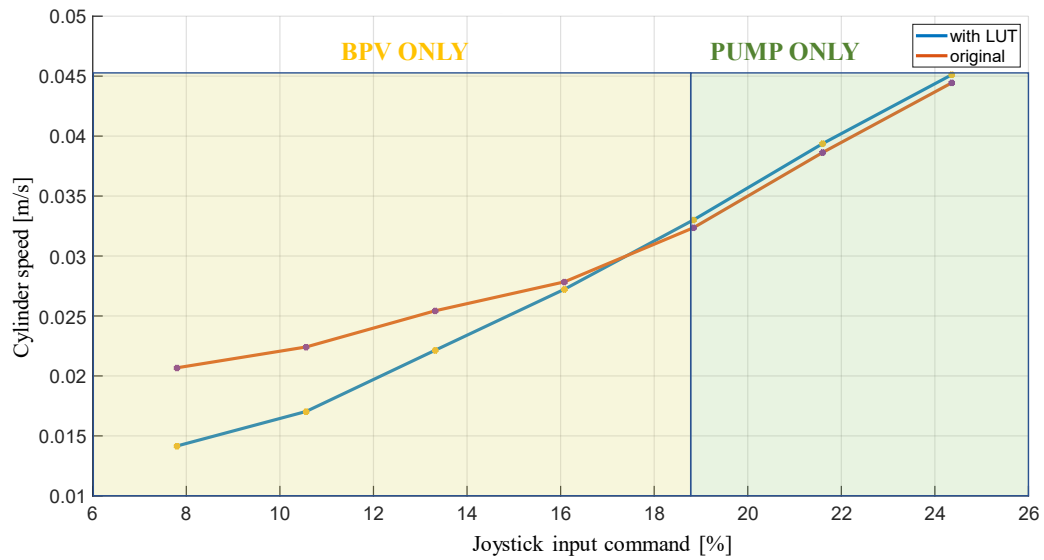


Figure 4.3: comparison between original control system and the new lookup table

## 4.2 Valve model development

The same experimental data acquired to create the map were also used to tune the valve model used in simulation. Image [4.4] shows how a two ways two positions proportional valve is modeled in Amesim, using the hydraulic components design library.

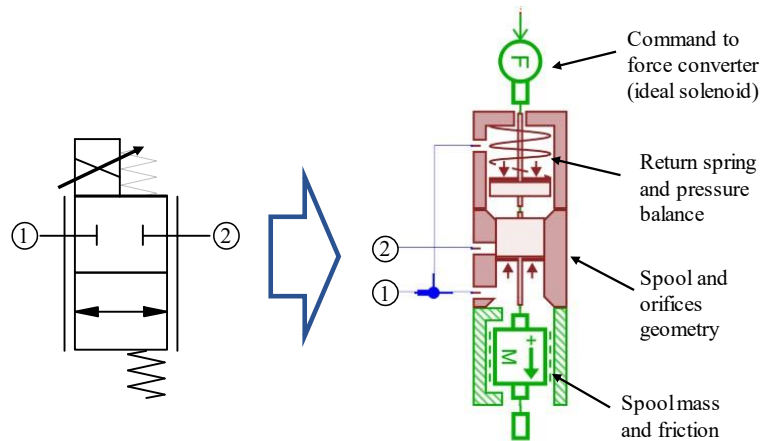


Figure 4.4: ISO schematic for the BPV and equivalent Amesim model

The flow area - spool position correlation can be described by equation 4.1, referring to figure [4.5] [S2019].

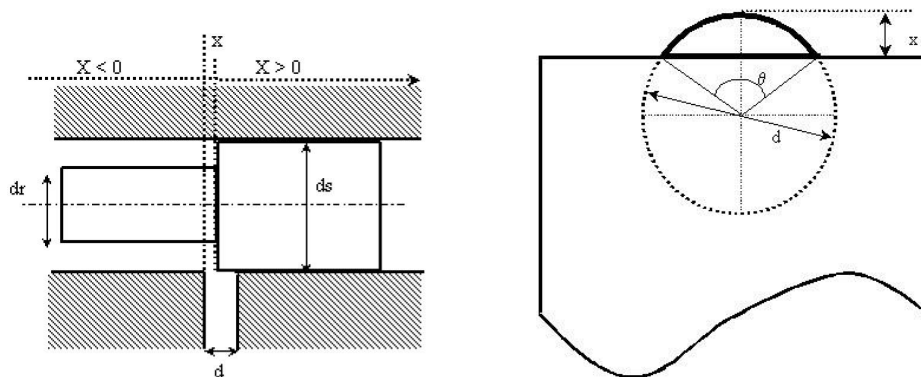


Figure 4.5: graphical representations of the parameters use to compute the flow area [S2019]

$$area = (\theta - \sin\theta) \frac{d^2}{8} \quad \text{where} \quad \theta = 2 \cdot \cos^{-1} \left( 1 - \frac{2x}{d} \right) \quad (4.1)$$

The hydraulic diameter is then computed as:

$$d_h = \frac{4 \cdot area}{perimeter} = \frac{8 \cdot area}{d \cdot \left( \theta + 2 \cdot \sin \frac{\theta}{2} \right)} \quad (4.2)$$

The flow force or jet force acting on the spool is always considered as valve closing force by the software, and described by equation 4.3.

$$F_{jet} = K_{jet} \cdot 2 \cdot C_d \cdot A \cdot dp \cdot \cos\theta \quad (4.3)$$

Where  $dp$  is the pressure differential,  $K_{jet}$  is a corrective coefficient usually set to 1 and tuned with experimental data, and  $\theta$  is the exit angle of the flow (also called jet angle), usually around  $69^\circ$  for spool valves. This force can be computed starting from the momentum equation presented in the first chapter, the full demonstration can be found in several textbooks such as V2021.

The parameters used to tune the valve model are: number of orifices and their diameter, critical flow number  $\lambda_{crit}$ , valve overlap (dead zone), maximum discharge coefficient and jet angle. Three datasets were used for three different pressures (26, 52 and 78 bar), with a valve voltage input from 3 to 5 V. A genetic algorithm with an initial population of 500 combinations was used to find the optimal values. A cost function was created to drive the algorithm, that minimizes the overall error and penalizes overfitting of a single dataset at the expense of the others (equation 4.4).

$$\int (e_{26}^2 - e_{52}^2)^2 + \int (e_{26}^2 - e_{78}^2)^2 + \int (e_{52}^2 - e_{78}^2)^2 \quad (4.4)$$

Where  $e_{26}$ ,  $e_{52}$ ,  $e_{78}$  are respectively the error between model and dataset at 26, 52 and 78 bar.

In the following table the valve parameters ranges, and the optimization results are shown:

Parameter	Range	Optimal value
Holes number	-	4
Holes diameter [mm]	4.5 → 6.5	5.38
Maximum $C_d$	0.611 → 0.8	0.657
Jet coefficient	0.9 → 1.1	0.92
Jet angle	0.65 → 0.69	0.69
Voltage-force gain	5 → 7	6.13
$\lambda_{crit}$	100 → 2000	695

*Table 4.1: BPV tuned parameters, tuning range and optimal result*

The fitting results are shown in figure [4.6], the valve shows good matching for every experimental set. The flow dataset relative to 78 bar constant pressure is less accurate because of experimental setup constraints. This validated valve will be part of the simulation model used in all the studies that will follow.

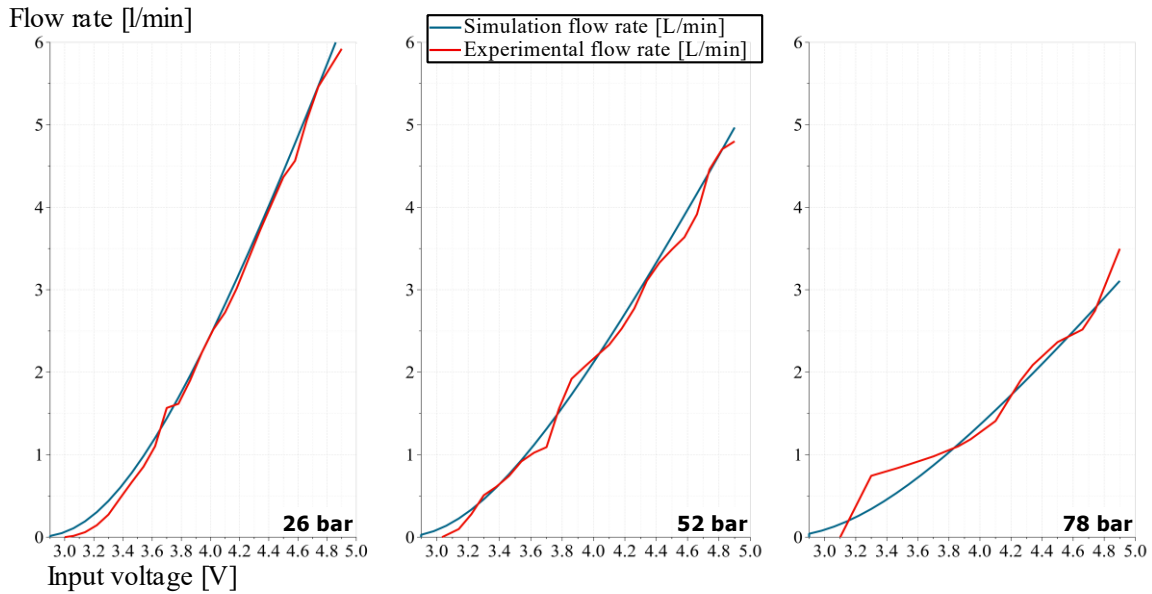


Figure 4.6: comparison between experimental data (red curves) and modeled valve behavior (blue curves) for different pressures.

For simulation purposes it was convenient to use an inverse model of the fitted valve to predict the exact flow rate, given pressure and input command. That was made inverting the same constitutive mentioned above in a Simulink model (figure[4.7]), then converted into an Amesim block (figure[4.8]). In that way it can be used as ideal flow mapping reference for the next simulations.

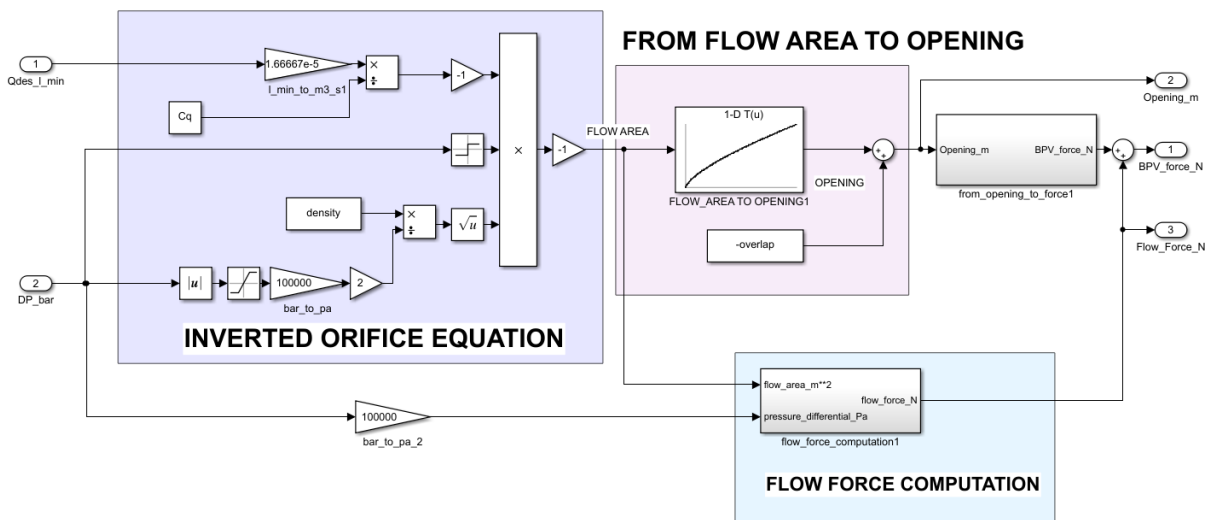


Figure 4.7: Simulink block diagram of the inverted valve

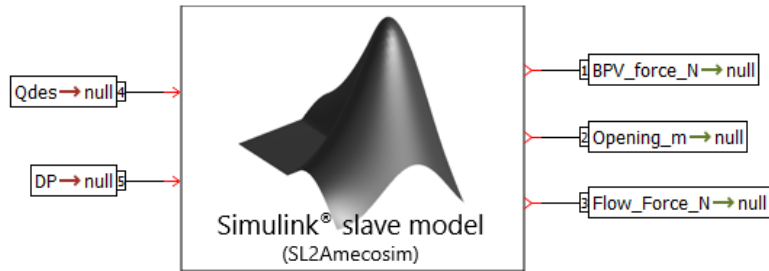


Figure 4.8: inverted valve from Simulink converted into an Amesim block (SL2Amecosim)

### 4.3 PI velocity control

The valve flow mapping results showed an acceptable velocity tracking even without feedback corrections. Static mapping is unfortunately unable to manage parameters variations or external disturbances. For that reason, a PI velocity control was implemented, using the position sensor derivative as velocity feedback. The possibility of using PID was rejected because of signal degradation due to double derivative.

The load generator present in the MPTR was too complex to be modeled and used for model-based control design, for this reason a heuristic approach was adopted. A PI controller (figure [4.9]) with clamping anti-windup was built in Simulink. The proportional ( $K_p$ ) and integral ( $K_i$ ) gains were added to the VeriStand user interface. In that way a real time manual tuning was possible.

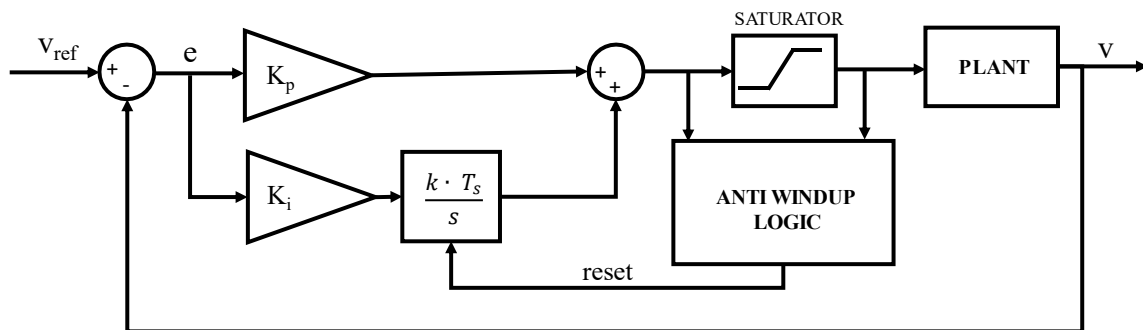


Figure 4.9: PI control with anti-windup scheme.

The Ziegler-Nichols tuning method was chosen, it consists in few simple steps:

- 1) Set  $K_i$  and  $K_p$  to 0
- 2) Gradually increase  $K_p$  and perform a step response every time. Save the value of  $K_p$  for which the system has consistent oscillations as  $K_u$  (ultimate gain). Measure the oscillation period and save it as  $T_u$  (ultimate period).

For a PI controller the Z-N method suggests a  $K_p = 0.45 \cdot K_u$  and a  $K_i = 0.54 \cdot \frac{K_u}{T_u}$ . Those gains were further improved manually until the best possible behavior was reached. The same approach was tried for both pump-driven (figure [4.10]) and valve-driven (figure [4.11]) states.

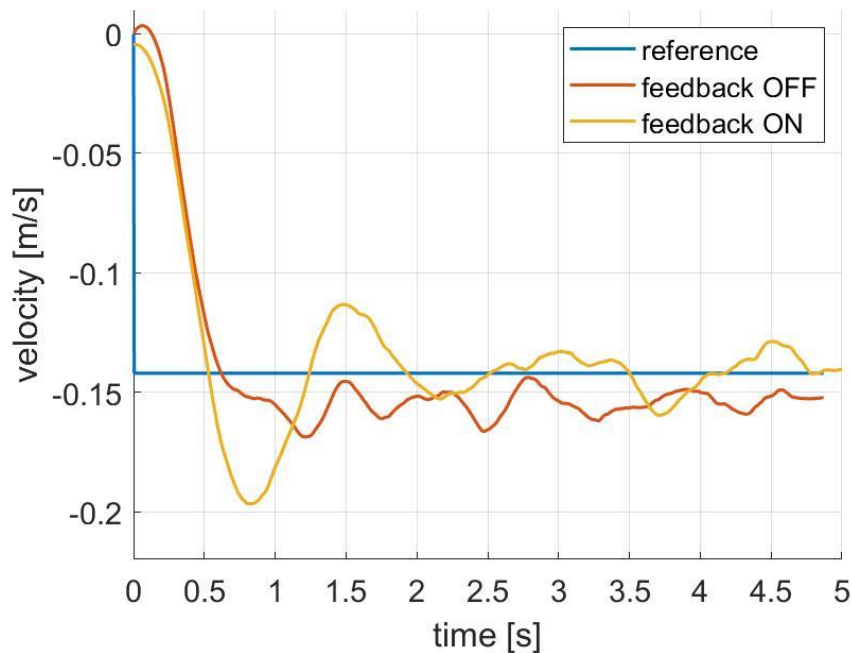


Figure 4.10: step response in high-speed assistive state (pump only), with and without the PI control

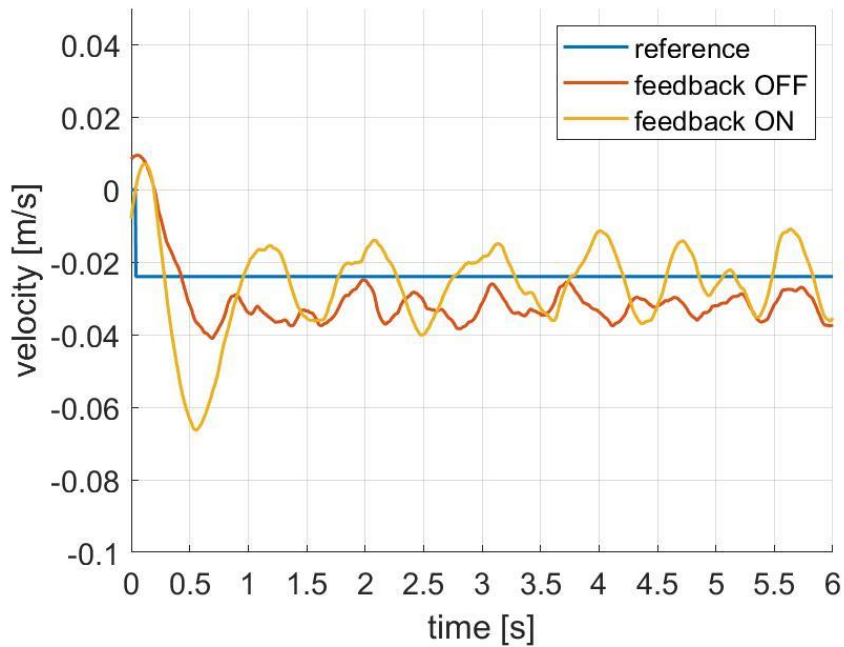


Figure 4.11: step response in low-speed assistive state (BPV only), with and without the PI control

The test, conducted with constant load, shows an oscillatory behavior and an overshoot increase. The cause comes from a combination of different reasons:

- Intrinsic low damping of the hydraulic system.
- Sensor noise, further amplified by the derivative, and phase delay introduced by necessary filtering.
- Load generator control interference with the implemented PI.

## 4.4 Considerations

The valve flow mapping led to the expected results, guaranteeing good tracking even without velocity feedback. PI control can decrease rise time and delete tracking error, but the absence of a derivative component inevitably contributes to worsening oscillations. From these considerations emerges the need for an increase in damping, the last chapter will be entirely focused on that issue.

The accurate velocity tracking priority is overshadowed by the damping requirements when considering the final EHA implementation. In the majority of hydraulic controls for mobile machines an open velocity control is the common choice. The reason is that the operator works as outer control loop, adjusting the joystick position to satisfy the speed requirement. Every inner control loop should then be fast enough to avoid interferences with the operator decisions. Data acquired from several tests, in several working conditions was used to improve and validate the non-linear model of the electro-hydraulic actuator (figure[4.12]). The Simulink-Amesim co-simulation ensured that the same control was running in both experimental and simulation environments.

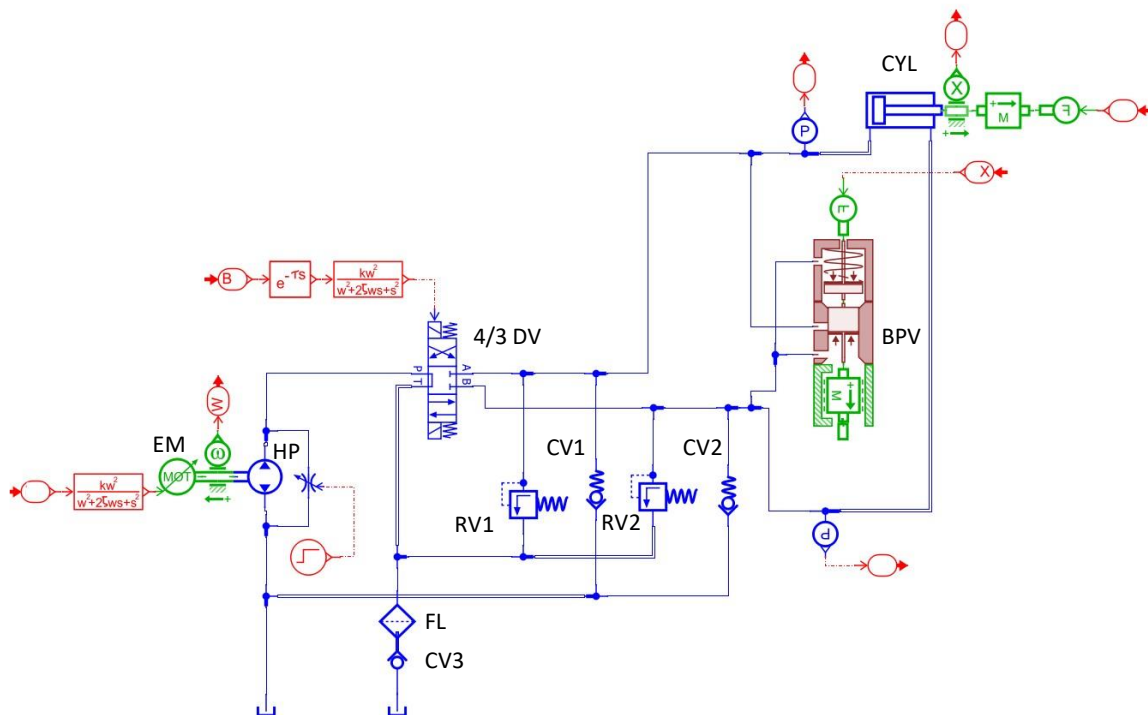


Figure 4.12: EHA modeled in Amesim environment (the circuit and the names of components refer to picture 1.1)

## 5. EHA on the machine (simulation)

In the previous chapter, valve information was extracted and the flow mapping decoupled flow control from load dependency. Then an empirical approach was tested to improve the system. This chapter will move on towards the final application and how to improve the dynamical behavior.

### 5.1 From the test rig to the real machine

To move further in the control development, it is necessary to adopt a model-based approach to forecast the EHA dynamic behavior once implemented in the reference machine. A characterization of the skid-steer mechanical part was developed in the past through experimental tests and converted into an Amesim model. A set of two EHA was added to this mechanical model (figure [5.1]), resulting in a complete actuator-load system.

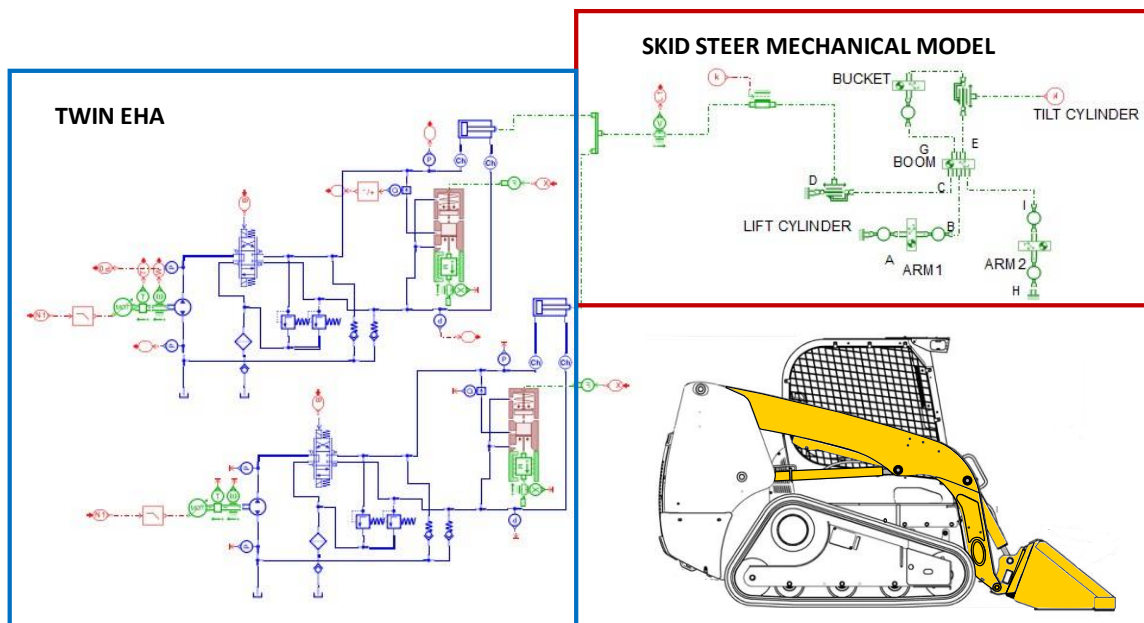


Figure 5.1: Simulation setup in Amesim environment, correspondent to the colored components on the skid-steer

The result is a complex system where several components act together to realize the desired output. Some of them are strongly non-linear and strictly dependent from unknown parameters and external variables. Identify all the parameters involved is not trivial, they are often hard and expensive to measure and the documentation, if present, usually only contains basic information. It is important to integrate different experimental datasets from the test rig, experience, and literature examples, to have a good guess of them.

The simulation is therefore used as a qualitative analysis, more than a quantitative one. Especially if the aim of the simulated model is to develop control strategies. Only the relevant dynamics must be considered.

The multi-domain nonlinear model created using Simcenter Amesim was used as a middle ground between the real system and the simplified linearized model that will be presented. It was used as a reference to quickly find out the most relevant agents and helped in choosing which non-linearities were irrelevant and which needed particular attention.

## 5.2 Model linearization

Linearization allows to study a nonlinear model with techniques proper of linear time invariant systems (LTI) and apply their relative control strategies. The result is only valid for certain operative ranges around the so-called linearization points. To have a complete idea of a nonlinear system behavior, several of these points are needed. In this study load and cylinder position were considered the most relevant time-variant parameters, the following rules resume the chosen linearization points:

- Two different load conditions, empty bucket and 1000kg load inside it.
- For each load different cylinder initial strokes, from 0.1 to 0.7 m.

The second step was the linear model definition, the following assumptions were made:

- The twin cylinders were converted into an equivalent single cylinder with doubled piston and rod areas.
- The skid-steer mechanical model was reduced into an equivalent load, composed by an equivalent mass  $m_{eq}$  and an equivalent viscous friction  $c_v$ .

- Only the piston side capacitance was considered, since the rod chamber is always connected to the tank, with low throttling connection [D2017]. Bulk modulus drops rapidly under 10 bar (figure [2.1]).
- The connection lines (if not significantly long) behave like a capacitance, due to the oil contained and the hose wall stiffness. Being the EHA a compact architecture, the connection lines capacitance was merged with the cylinder's one, resulting in a unique equivalent capacitance  $C_{H,eq}$  [K2012].
- Two inputs were considered, inlet flow  $Q_{in}$  and external load force  $F_{in}$ .
- The model is restricted to resistive extension and assistive retraction, since when implemented on the machine the EHA works almost always in those states.

The result of the above considerations is graphically presented in picture [5.2].

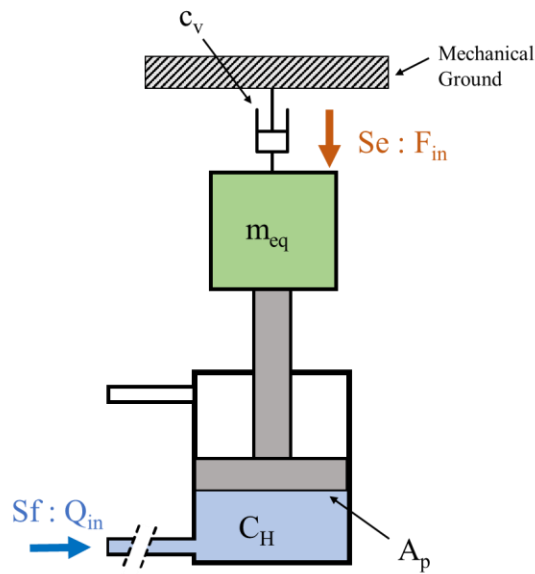


Figure 5.2: Graphical representation of the simplified linearized model

Applying the second Newton Law to the cylinder the following force balance is computed:

$$m_{eq} \cdot \ddot{x} = p_P \cdot A_P - c_v \cdot \dot{x} - F_{in} \quad (5.1)$$

Where  $\dot{x}$  is the cylinder velocity and  $\ddot{x}$  is acceleration. In the Laplace domain it can be written as:

$$m_{eq} \cdot s \cdot \dot{x} = p_P \cdot A_P - c_v \cdot \dot{x} - F_{in} \quad (5.2)$$

$$\dot{x} = \frac{A_P \cdot p_P - F_{in}}{(c_v + m_{eq} \cdot s)} \quad (5.3)$$

Applying the pressure build up equation (2.24) to the cylinder piston side:

$$\dot{p}_P = \frac{1}{C_H} \cdot \left( Q_{in} - \frac{\partial V}{\partial t} \right) = \frac{1}{C_H} \cdot (Q_{in} - A_P \cdot \dot{x}) \quad (5.4)$$

In the Laplace domain:

$$p_P = \frac{1}{C_H \cdot s} \cdot (Q_{in} - A_P \cdot \dot{x}) \quad (5.5)$$

Merging (5.3) and (5.5) the piston side pressure  $p_P$  can be written as function of the two inputs:

$$p_P = Q_{in} \cdot \frac{(c_v + m_{eq} \cdot s) \cdot K_H}{c_v \cdot s + m_{eq} \cdot s^2 + A_P^2 \cdot K_H} + F_{in} \cdot \frac{A_P \cdot K_H}{c_v \cdot s + m_{eq} \cdot s^2 + A_P^2 \cdot K_H} \quad (5.6)$$

Where:

$$1/C_H = K_H \quad (5.7)$$

In a similar way the cylinder velocity  $\dot{x}$  can be computed:

$$\dot{x} = Q_{in} \cdot \frac{A_P \cdot K_H}{c_v \cdot s + m_{eq} \cdot s^2 + A_P^2 \cdot K_H} + F_{in} \cdot \frac{s}{c_v \cdot s + m_{eq} \cdot s^2 + A_P^2 \cdot K_H} \quad (5.8)$$

Starting from those analytical transfer functions, the numerical parameters of the linearization  $K_H$ ,  $c_v$ ,  $m_{eq}$  and the steady state equivalent force (due to gravity) were extracted. That was made by fitting the linearized model with the nonlinear one realized in Amesim. Pictures [5.3, 5.4] shows the differences between the two model with a bucket load of 1000 kg and a cylinder initial position of 0.18 m. In the nonlinear model the pressure slowly decreases with the time because of the cylinder extension, and the consequent change in force balance. That dynamic is so slow that will not effect the next studies.

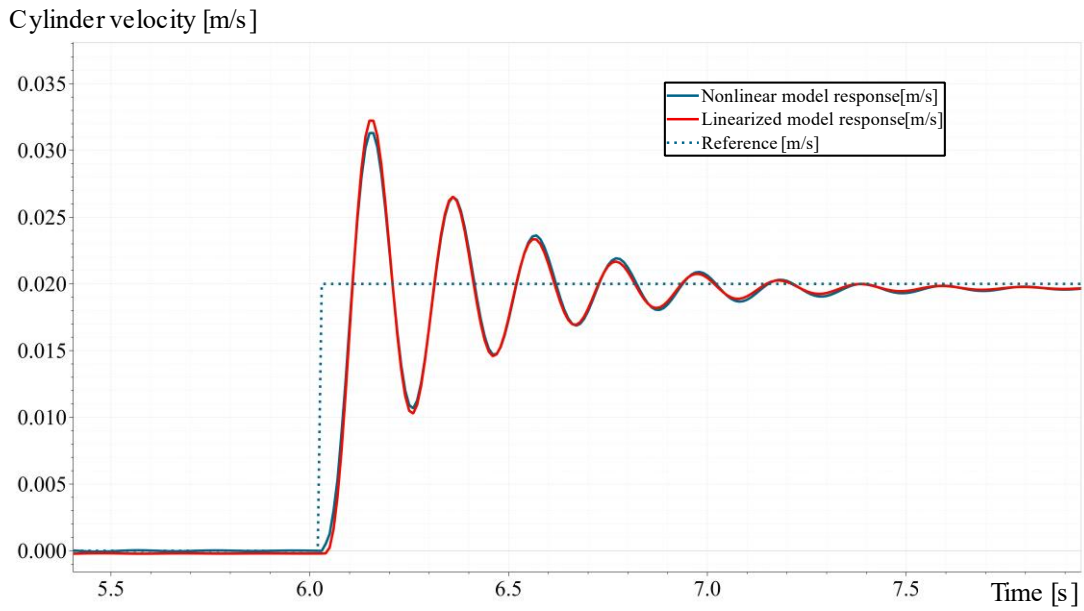


Figure 5.3: Velocity step response, linearized and nonlinear model (Amesim) compared.

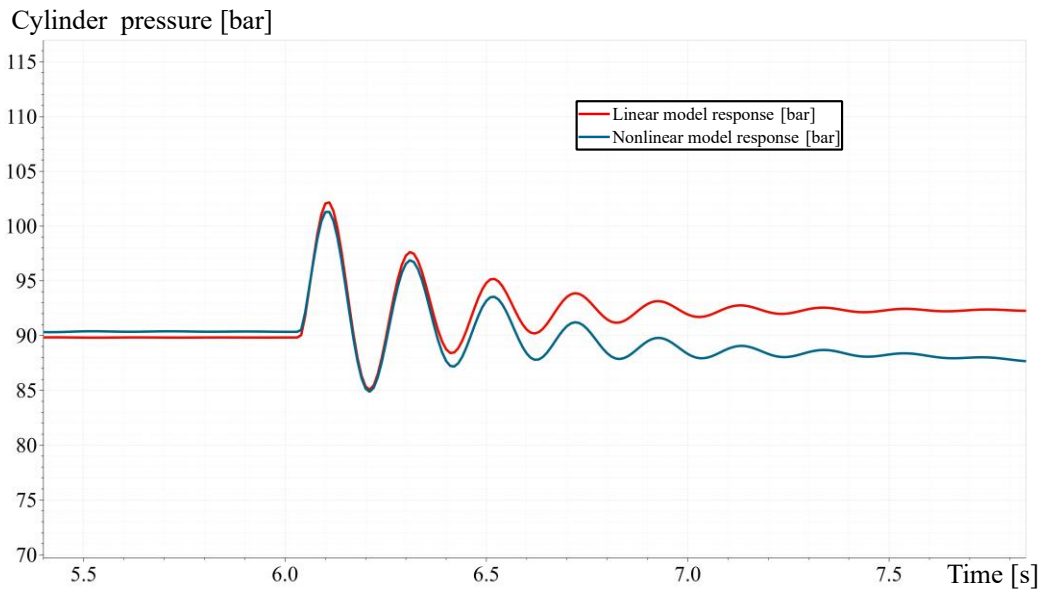


Figure 5.4: Pressure in velocity step response, linearized and nonlinear model (Amesim) compared.

Putting together all the linearized models an analysis was done in terms of natural frequency [figure 5.5] and damping [figure 5.6]. As predicted in chapter 2, the system presents low damping for every working condition, tending to get worse with high loads. The natural frequency decreases with the load, and its minimum is reached in full extension. This characteristic can be an advantage: as explained later, the effectiveness of the oscillation reducing control strategy is strictly related to the relative difference between controlled system and control valve respective natural frequencies. The slower is the system the most effective the electronic oscillation damping is.

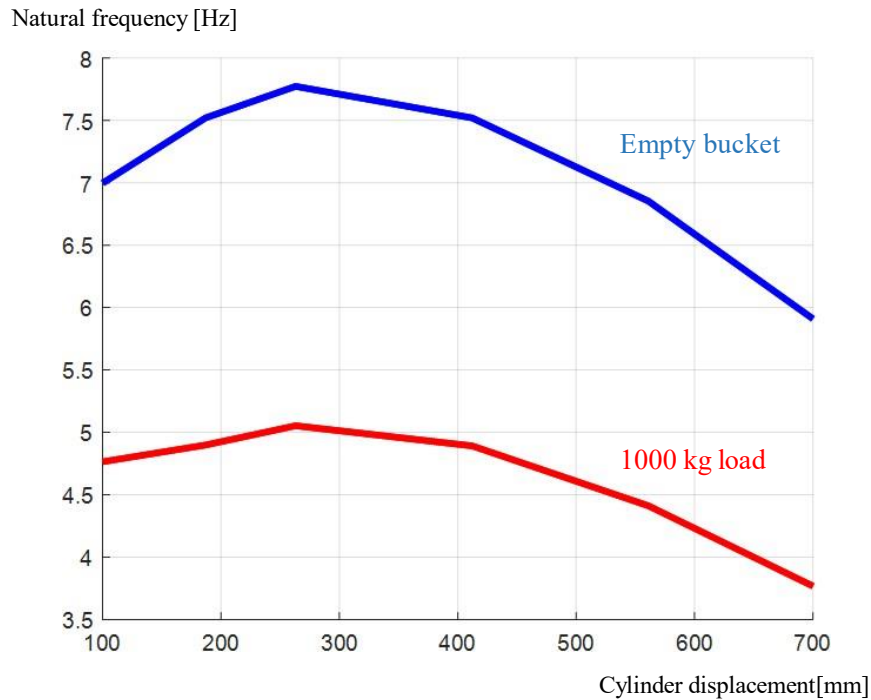


Figure 5.5: Natural frequency for the different load conditions, varying the cylinder extension

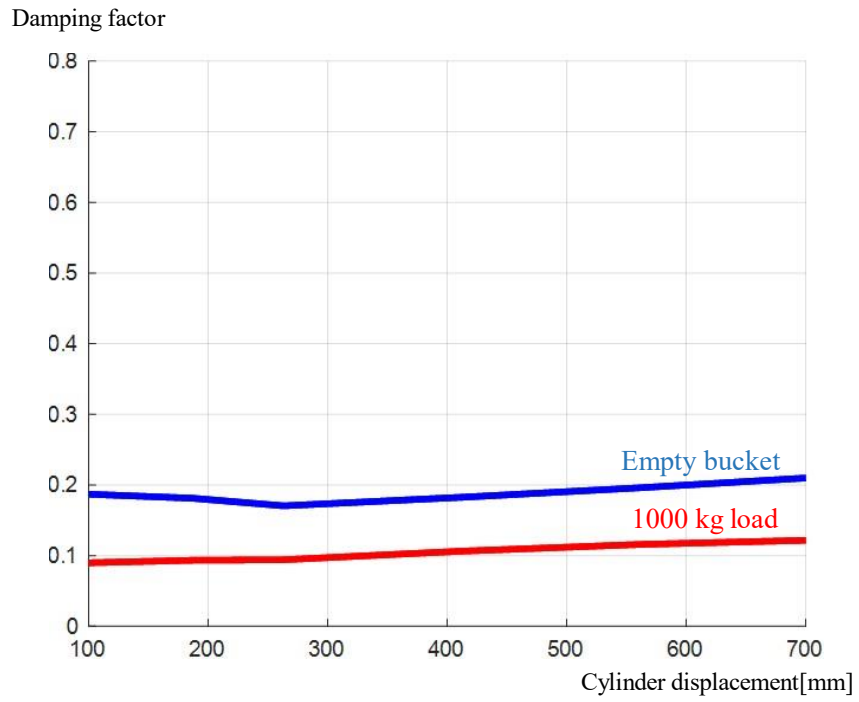


Figure 5.6: Damping factor for the different load conditions, varying the cylinder extension. Its value is critically low and far from the ideal values for a well damped system (0.7).

### 5.3 Control development: Pressure Feedback

The previous linear analysis proved the expected dynamic EHA behavior when implemented on the real machine. The low damping not only impacts operator comfort but also safety. Excessive oscillations can lead to instability and tipping if the center of gravity is too high.

The implementation of pressure feedback to improve damping in hydraulic systems was extensively discussed for various applications: [D2017] uses it in an excavator with independent metering architecture, [Za2013] applied it to a SANDVIK mining machine, [M2019] to a CASE 721f wheel-loader. Pedersen and Andersen [P2018] gave an analytical overview of different pressure feedback strategies, together with a method to tune the control parameters. [D2017] Describes the pressure feedback damping effect by the correlation with pressure and cylinder velocity derivative.

Among all the different combinations a high pass filtered pressure feedback was chosen (picture [5.7]). The HPF deletes the steady state pressure value, enabling the feedback only when high frequency oscillation occurs.

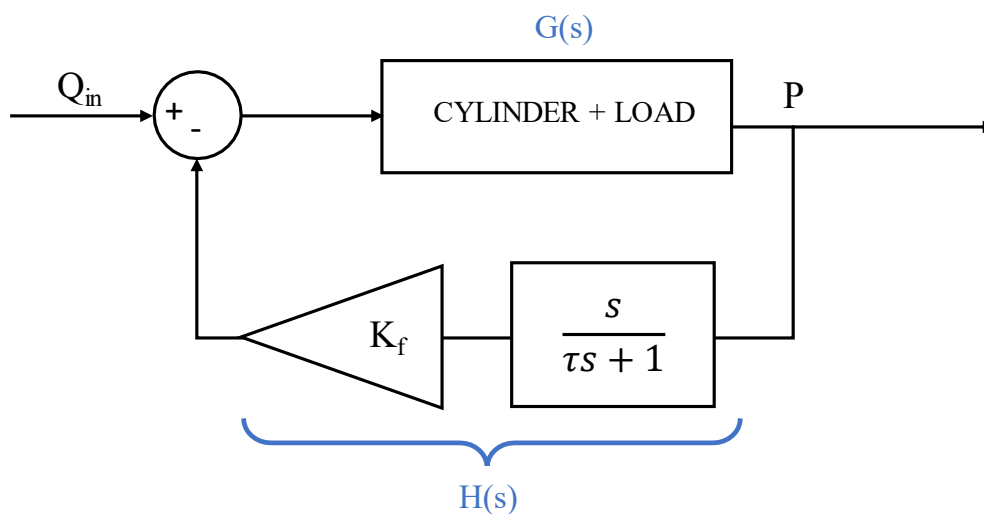


Figure 5.7: High pass filtered pressure feedback control scheme

The root locus analysis was used to study the effect of the feedback parameters variation on the dynamic behavior. That is done by plotting all the different roots of the closed loop transfer function (5.9).

$$\frac{y}{u} = \frac{G(s)}{1 + G(s)H(s)} \quad (5.9)$$

From (5.6), considering only  $Q_{in}$  as input ( $F_{in}$  is considered constant) the transfer function  $G(s)$  is computed:

$$G(s) = \frac{\dot{x}}{Q_{in}} = \frac{(c_v + m_{eq} \cdot s) \cdot K_H}{c_v \cdot s + m_{eq} \cdot s^2 + A_P^2 \cdot K_H} \quad (5.10)$$

$H(s)$  is the feedback transfer function:

$$H(s) = K_f \cdot \frac{s}{\tau s + 1} \quad (5.11)$$

The closed loop poles are the solution of the equation (5.12).

$$1 + G(s)H(s) = 0 \quad (5.12)$$

The root locus is the plot in the s-plane of every solution found changing a parameter on the transfer function. That was done in MATLAB using the `rlocus(GH)` function.

Looking at  $H(s)$  (equation 5.11) two different parameters can be tuned: the feedback gain  $K_f$  and the filter time constant  $\tau$ . Picture [5.7] shows the root locus for a pressure feedback system example (1000 kg load and 0.19 m cylinder initial displacement) with variable  $K_f$ . The different curves are plotted for  $\tau = j/\omega_n$  with  $j$  going from 1.2 to 2.8 and  $\omega_n$  indicating the open loop transfer function ( $G(s)$ ) natural frequency.

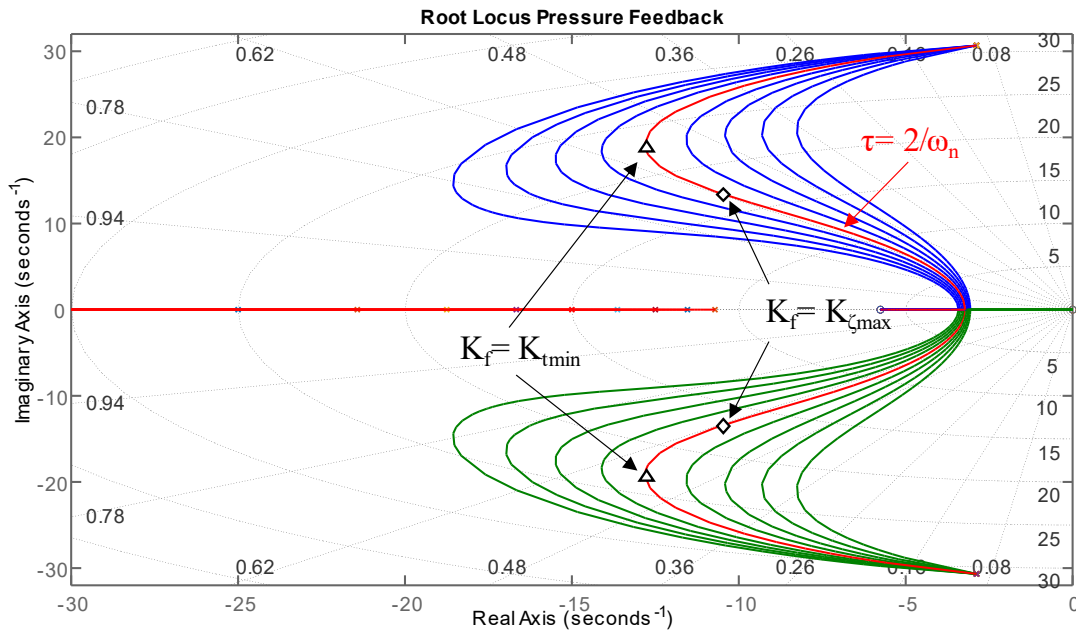


Figure 5.8: Pressure feedback root locus, each curve has a different  $\tau$ , moving along a curve towards the real axis  $K_f$  increases.

Since  $\tau$  can be related to the system natural frequency it is the first to be tuned. From the root locus can be assumed that the longest is the time constant, the highest is the achievable damping. To set a reasonable max length bound it is important to think about the real application of the system: having a filter that allows most of the frequencies will let the feedback operate even in unwanted conditions and interfere with the operator's will. A limited  $\tau$  value will ensure that only the high frequency unwanted oscillations are feed back. A deeper study on the interference between  $\tau$  and operator command can be done

once the EHA is implemented in the machine. In this paper the  $\tau$  value was chosen as  $2/\omega_n$  (red curve in picture [5.7]).

Once  $\tau$  is set,  $K_f$  can be directly extracted from the root locus plot. Along the root path, two relevant values were considered:

- A  $K_{\zeta_{max}}$  that is the gain corresponding to the maximum achievable damping.
- A  $K_{t_{min}}$  that is the gain corresponding to the fastest achievable transient decay.

As suggested by [P2018] every value between those limits is considered a good choice.

Following those guidelines, a gain scheduling was implemented, the result applied to the 1000 kg load condition is shown in picture [5.9]. The control successfully increases the damping factor, well above the original open-loop system. The final value is close to the optimal damping objective adopted by [D2017].

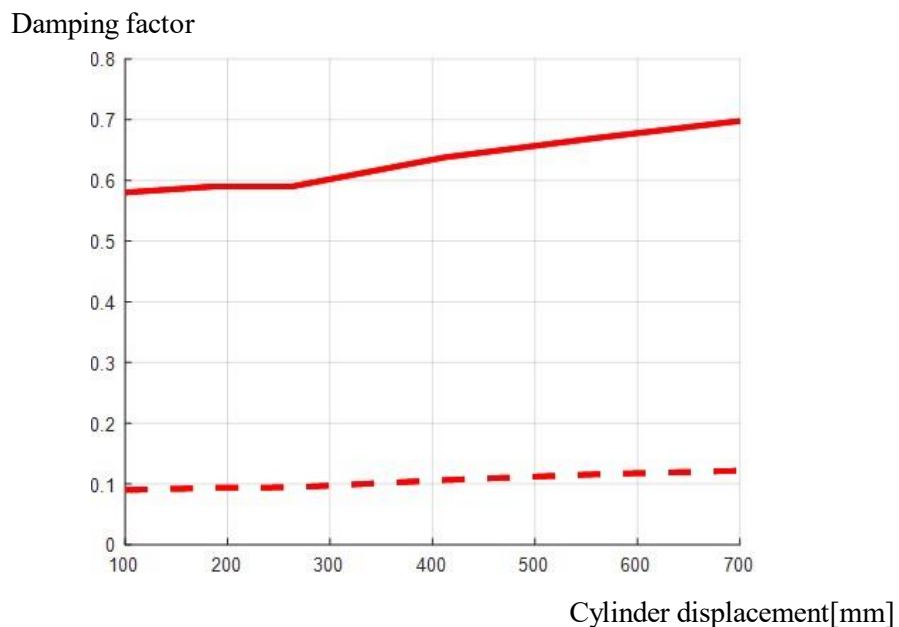


Figure 5.9: Damping factor comparison for the 1000 kg load condition, the dashed line represents the original open-loop system, the solid one is the result of the new pressure feedback.

The control system was then implemented in the nonlinear model built in Amesim, showing a good level of accuracy (figure[5.10]).

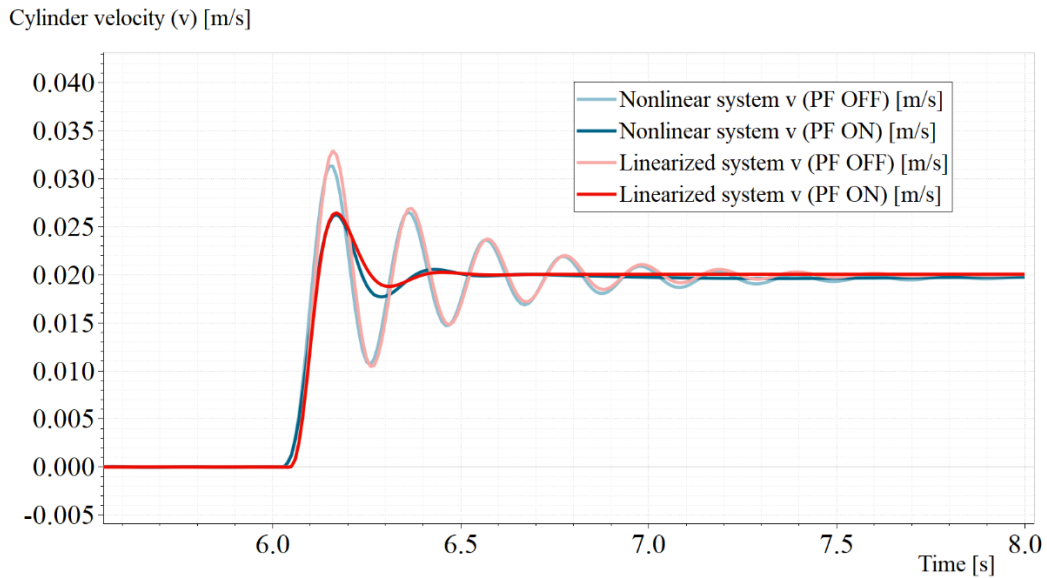


Figure 5.10: comparison between pressure feedback ON/OFF for nonlinear model (Amesim) and linearized model.

The last test was performed by including the valve dynamics as a second order system. The figure [5.11] shows how the valve natural frequency influences the pressure feedback behavior. The result is a gradual performance degradation when the valve natural frequency approaches the open loop system frequency.

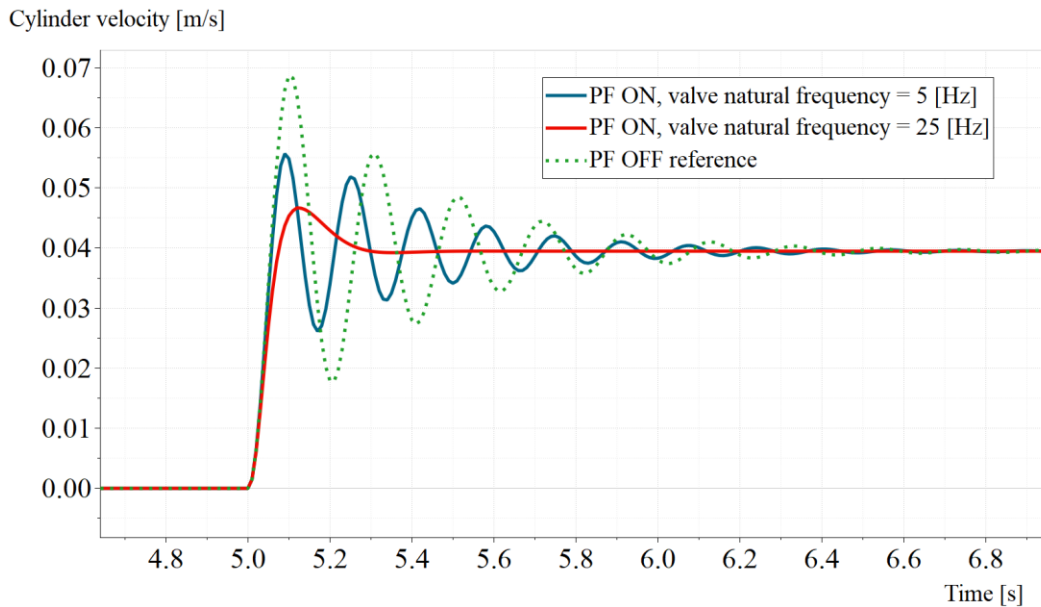


Figure 5.11: Pressure feedback performance with different valve natural frequencies

## 5.4 Ride control preliminary study

In the previous chapter an active method was introduced to increase the EHA damping in the main working states: resistive extension and assistive retraction. In those states the BPV was always able to connect the high-pressure chamber of the cylinder to the low-pressure line, if requested by the pressure feedback, realizing in that way the desired dynamic oscillation reduction.

When the user is not acting on the joystick the directional valve stays closed (idle condition). It means that the cylinder is completely isolated from pump and tank. That situation makes pressure feedback ineffective. In the original skid-steer schematic a passive ride control system was already implemented, indicating the need of a system to reduce oscillatory effects from external forces during the ride (figure [5.12]).

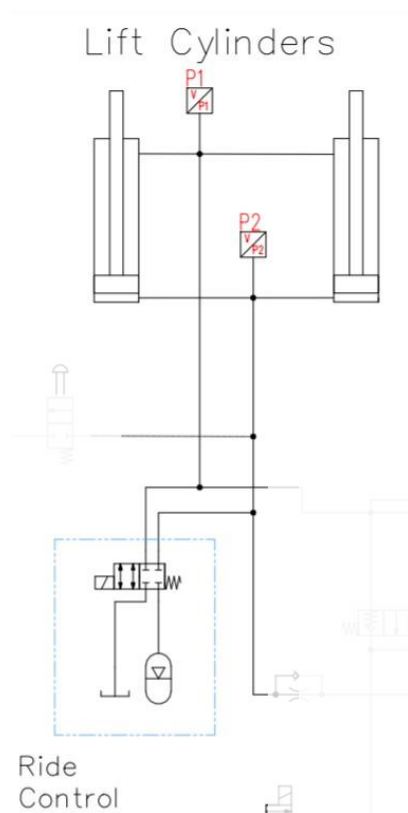


Figure 5.12: in the original skid-steer system an on-off valve activates a passive ride control circuit.

The original solution uses a valve to connect the rod side of the cylinders to tank and the piston side, which is holding the load, to an accumulator.

When implementing the EHA, a solution could be to replace the directional tandem center valve with a different one, always able to provide low pressure connection (figure[5.13]), and, in that way, always allow pressure feedback to operate.

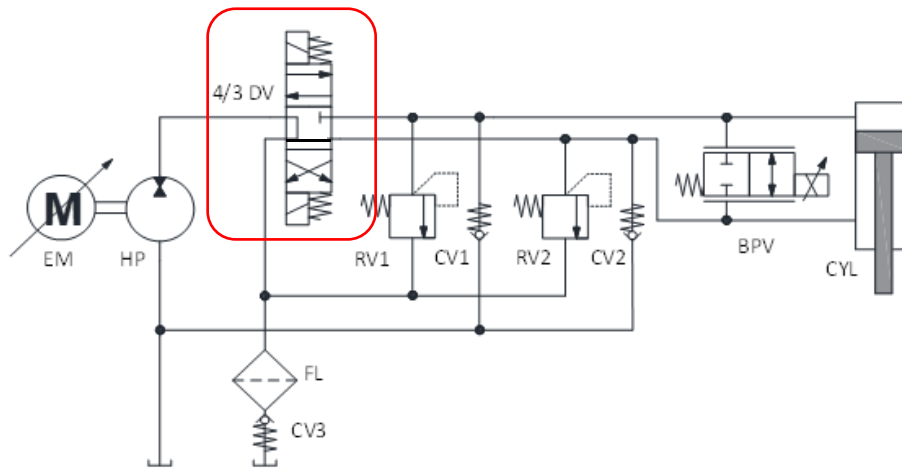


Figure 5.13: Directional valve replacement to allow pressure feedback in idle condition

That solution could lead to additional problems such as permanent rod chamber connection to the tank even in unwanted conditions. Furthermore, if the pressure feedback operates in idle condition, a position control should consider the boom lowering introduced by wasted flow.

To avoid circuit modifications and an increase of overall system complexity, a feasibility study to implement a ride control by exploiting the BPV was conducted. The Bond Graph approach [appendix A] was used to model an equivalent linear system of the idle condition, considering the bypass valve as a variable resistance. A graphical representation is shown in figure[5.14].

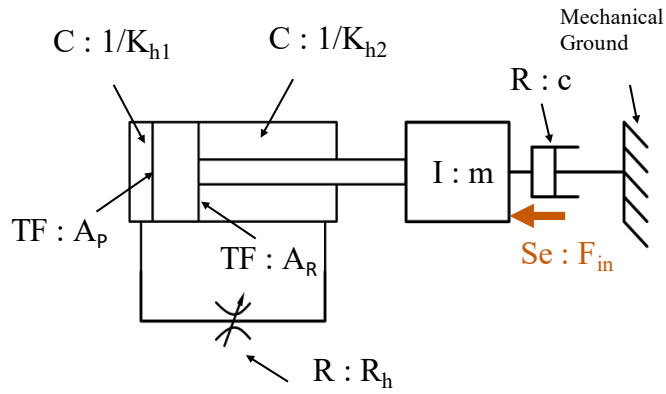


Figure 5.14: simplified system in idle position (4/3 DV closed)

The resulting Bond Graph is shown in figure [5.15]

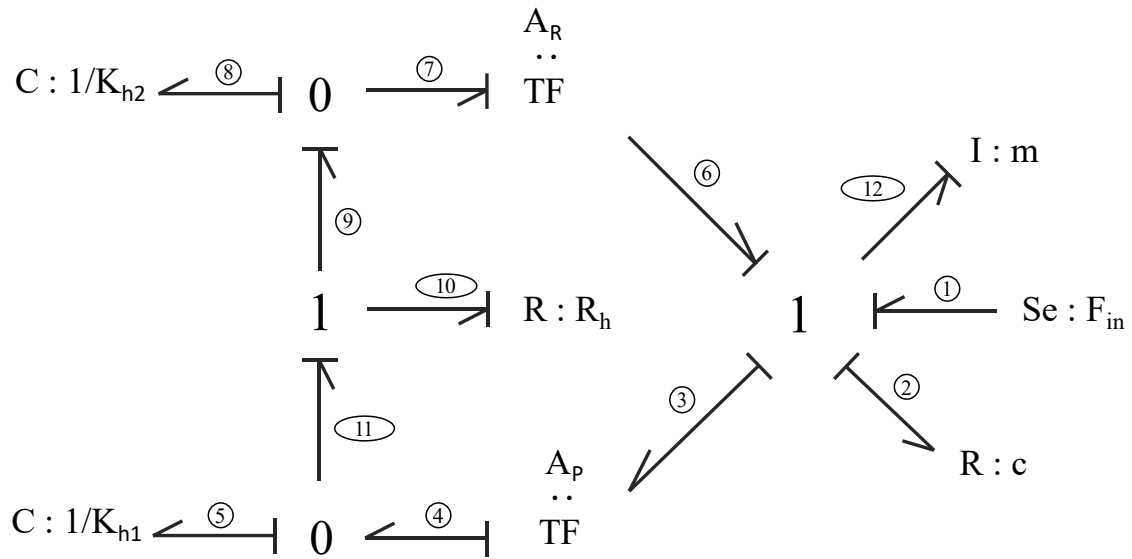


Figure 5.15: Simplified system idle position Bond Graph

Starting from the Bond Graph a systematic computation led to the following state space:

$$\begin{bmatrix} \dot{q}_5 \\ \dot{q}_8 \\ \dot{p}_{12} \end{bmatrix} = \begin{bmatrix} -\frac{K_{h1}}{R_h} & \frac{K_{h2}}{R_h} & \frac{A_P}{m} \\ \frac{K_{h1}}{R_h} & -\frac{K_{h2}}{R_h} & -\frac{A_R}{m} \\ -A_P \cdot K_{h1} & A_R \cdot K_{h2} & -\frac{c}{m} \end{bmatrix} \cdot \begin{bmatrix} q_5 \\ q_8 \\ p_{12} \end{bmatrix} + \begin{bmatrix} 0 \\ 0 \\ 1 \end{bmatrix} \cdot F_{in} \quad (5.13)$$

Is important to recall that  $p_{12}$  is a generalized momentum, while  $q_5$  and  $q_8$  are generalized displacements [Appendix A]. The choice of this symbols can be confusing, for that reason, in that paragraph the pressure will be presented as uppercase symbol  $P$ .

The following output matrix was chosen:

$$\begin{bmatrix} P_1 \\ P_2 \\ v_{cyl} \\ Q_{valve} \end{bmatrix} = \begin{bmatrix} K_{h1} & 0 & 0 \\ 0 & K_{h2} & 0 \\ 0 & 0 & \frac{1}{m} \\ \frac{K_{h1}}{R_h} & -\frac{K_{h2}}{R_h} & 0 \end{bmatrix} \cdot \begin{bmatrix} q_5 \\ q_8 \\ p_{12} \end{bmatrix} \quad (5.14)$$

Where  $P_1$  is the piston chamber pressure,  $P_2$  is the rod chamber pressure,  $v_{cyl}$  the cylinder speed and  $Q_{valve}$  is the flow through the valve.

The equation (5.15) was used in MATLAB to convert the state space model into the four transfer functions.

$$\mathbf{G}(s) = \mathbf{C} \cdot (s \cdot \mathbf{I} - \mathbf{A})^{-1} \cdot \mathbf{B} \quad (5.15)$$

A Bode diagram of the transfer function connecting  $P_1$  to  $F_{in}$  to was then plotted for various resistance values. In figure 5.14 the results for the optimum value  $R_{h,opt}$  and the two resistance extremes:

$$R_{high} = 10 \cdot R_{h,opt} \quad ; R_{low} = 0.1 \cdot R_{h,opt}$$

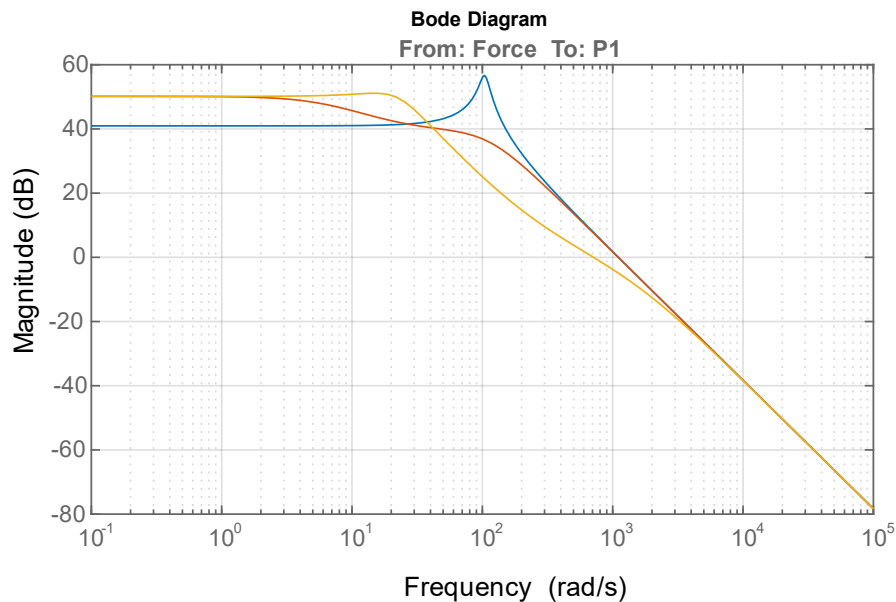


Figure 5.16 bode plot of the Force to Pressure transfer function, the orange curve corresponds to  $R_{h,opt}$  the yellow one corresponds to  $R_{low}$  and the blue one is the reference ( $R_{high}$ ).

From figure [5.14] some considerations can be taken: With high resistance the chambers are not connected together, that implies the highest oscillation. With low resistance the chambers are connected, resulting in an increased capacitance and therefore a better damping, the only relevant dissipative component is the load viscous friction. In the middle an optimal resistance value can be found, that contributes to the power dissipation and increases the damping to the maximum achievable with this solution.

## 5.5 Considerations

The pressure feedback introduction drastically increased the system damping. The damping coefficient goes from the original 0.1 to 0.6, limiting the oscillation in a single, reduced, overshoot. The same performance is validated even in the nonlinear simulation. The valve natural frequency has an important role on the pressure feedback effectiveness. The used BPV is supposed to be fast enough to not affect the performance.

The ride control solution initial results confirm an improved oscillation damping than the original configuration, but a more detailed research is needed to confirm it in the real application. It is important to consider that in the open BPV configuration the pressure in both chambers is equalized to a value that is higher than the one measured with separated chambers. That will restrict the operative ranges to empty bucket or low loads.

## 6. Conclusions

Previous studies on this novel EHA architecture proved reliability and high efficiency performance, making the system highly competitive with respect to the one originally implemented on the machine, in terms of power consumption.

This thesis proved that the EHA can compete with the original system also on the dynamic field, with proved comfort, safety, and stability.

The bypass valve, main objective of this work, is now not only limited on few working states, just to limit cylinder velocity. Its usage is now extended to all the working conditions and act together with the pump to synergically control the system. The flow mapping smoothed the switch between the two drivers improving accuracy and comfort. The pressure feedback implementation exploits the fast response of the valve to improve system damping. The ride control tries to use the BPV to reduce oscillations from external agents even in idle condition.

The model-based approach to model both controllers and embedded software not only helped in the development of the present study but will be the base for every future test and improvement.

## 7.Future work

This research has given rise to numerous ways of improvement, and future work ideas:

- The developed controllers should be tested with the real load and real working conditions to fully validate the simulation results.
- The valve dynamic response can be characterized in a more accurate way, using an ad-hoc test rig.
- The valve mapping can be automatically updated during the time, by collecting voltage, pressure, and position data. In that way the mapping can be adapted to system aging, and even used to forecast failures.
- A better velocity controller and better sensors can be adopted to achieve an improved reference tracking.
- Since a twin EHA set will act on the same load at the same time, a supervisory control can be developed to synchronize them.

# References

- [D2007] Dragan V. Lazić, Milan R. Ristanović. (2007) Electrohydraulic thrust vector control of twin rocket engines with position feedback via angular transducers, *Control Engineering Practice*, Volume 15, Issue 5, 2007, Pages 583-594,
- [D2017] Ding, R.; Xu, B.; Zhang, J.; Cheng, M. (2017). Self-tuning pressure-feedback control by pole placement for vibration reduction of excavator with independent metering fluid power system. *Mechanical Systems and Signal Processing* 92:86-106.
- [J2003] Jelali, M.; Kroll, A. (2003). *Hydraulic Servo-systems. Modelling, Identification and Control*. Springer.
- [K2012] Karnopp, D.C.; Margolis, D.L.; Rosenberg, R.C. (2012). *Modeling, Simulation, and Control of Mechatronic Systems*, Fifth Edition. Wiley.
- [L1965] Lichtarowicz, A.; Duggins, R. K.; Markland, (1965). Discharge Coefficients for Incompressible Non-Cavitating Flow through Long Orifices. *Journal of Mechanical Engineering Science* 7:210-219.
- [M2019] Madau, R. ; Vacca, A. (2019) Active Ride Control for Construction Machines Based on Pressure Feedback. *Proceedings of the ASME/BATH 2019 Symposium on Fluid Power and Motion Control*. ASME/BATH 2019 Symposium on Fluid Power and Motion Control. Longboat Key, Florida, USA. October 7–9, 2019. V001T01A021. ASME.
- [M2020] Manring, N. D.; Fales, R.C. (2020). *Hydraulic control Systems*. Wiley.
- [P2018] Pedersen, H. C.; Andersen, T. O. (2018). Pressure Feedback in Fluid Power Systems—Active Damping Explained and Exemplified. *IEEE Transactions on Control Systems Technology*, 26(1), 102-113. doi: 10.1109/TCST.2017.2650680

- [Q2020] Qu, S. ; Fassbender, D.; Vacca, A.; Busquets, E. (2020). Formulation, Design and Experimental Verification of an Open Circuit Electro-Hydraulic Actuator. Conference: 2020 IEEE Global Fluid Power Society PhD Symposium (GFPS).
- [S2019] Siemens Industry Software, inc. (2019). Simcenter Amesim Reference Manual.
- [T2019] Tonoli, A. (2019). Modeling and Simulation of Mechatronic systems lectures notes Polytechnic University of Turin
- [Vi1980] Viersma, T.J. (1980). Analysis, Synthesis and Design of Hydraulic Servosystems and Pipelines. Elsevier.
- [V2021] Vacca, A.; Franzoni, G. (2021). Hydraulic Fluid Power: Fundamentals, Applications, and Circuit Design. Wiley.
- [W1954] Wuest W (1954) Stromung durch Schlitz- und Lochblenden bei kleinen Reynolds-Zahlen. Ing Arch 22:357-367
- [Za2013] Zaev, Emil ; Rath, Gerhard ; Kargl, Hubert. (2013). Energy Efficient Active Vibration Damping. 355-364. 10.3384/ecp1392a35.
- [Z2018] Zhang, Q. (2018). Basics of Hydraulics Systems, Second edition. CRC Press.

# Appendix: Bond Graph

In this appendix a brief introduction of Bond Graphs will be presented, it is not a complete guide but will be helpful in understanding how to interpret the models present in this paper. If interested please refer to [K2012].

A bond graph (figure[A.1]) is a standard graphical representation of dynamic mechatronic systems, based on power exchange between components. It is a systematic approach that follows common rules, regardless of the involved components. Bond graphs are used as starting points to develop state-space models.

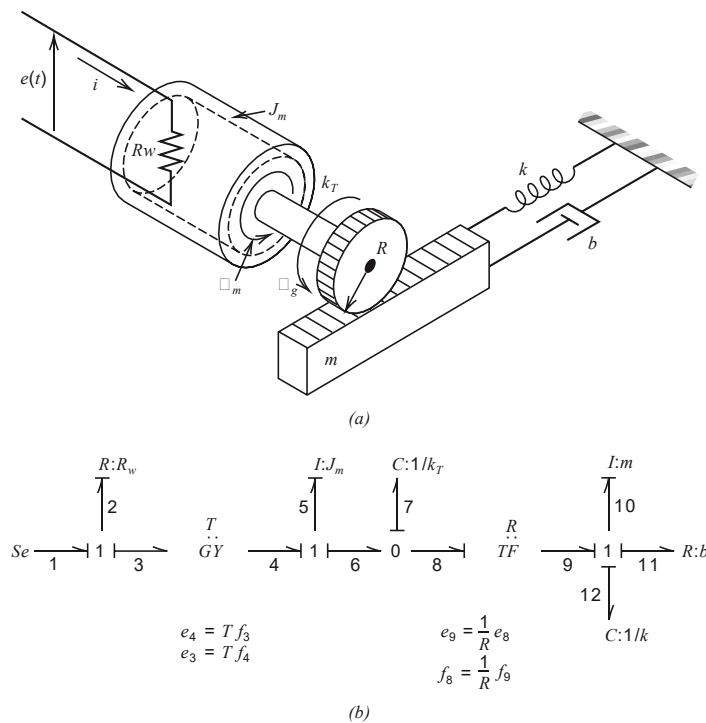


Figure A.1: from a mechatronic system to a Bond Graph [K2012]

Bond graphs are based on generalized power variables: **effort** and **flow**, the product between them is the generalized power. Two additional variables, called energy variables, describe the system evolution during the time: **generalized momentum  $p(t)$**  and

**generalized displacement  $q(t)$ .** Their relationship with the power variables is described with integral or derivative relations (equations A.1 and A.2).

$$p(t) \equiv \int e(t)dt; \quad \frac{dp(t)}{dt} = e(t) \quad (\text{A.1})$$

$$q(t) \equiv \int f(t)dt; \quad \frac{dq(t)}{dt} = f(t) \quad (\text{A.2})$$

The following table shows the correspondence between the generalized variables and the standard variables of each domain [K2012, T2019].

	<b>f</b> <i>flow</i>	<b>e</b> <i>effort</i>	<b>q = ∫f dt</b> <i>generalized displacement</i>	<b>p = ∫e dt</b> <i>generalized momentum</i>
<b>Electric</b>	i <i>current</i>	e <i>voltage</i>	q = ∫i dt <i>charge</i>	λ = ∫e dt <i>flux linkage</i>
<b>Mechanical (translation)</b>	v <i>velocity</i>	f <i>force</i>	x = ∫v dt <i>displacement</i>	p = ∫f dt <i>momentum</i>
<b>Mechanical (rotation)</b>	ω <i>angular velocity</i>	T <i>torque</i>	θ = ∫ω dt <i>angular displacement</i>	b = ∫T dt <i>angular momentum</i>
<b>Hydraulic</b>	Q <i>volume flow</i>	P <i>pressure</i>	V = ∫Q dt <i>volume</i>	p <sub>p</sub> = ∫P dt <i>pressure momentum</i>

**Single port components** represent the classical lumped parameter resistances, capacitances, and inductances.

The resistance relate effort and flow and is considered a dissipative element.

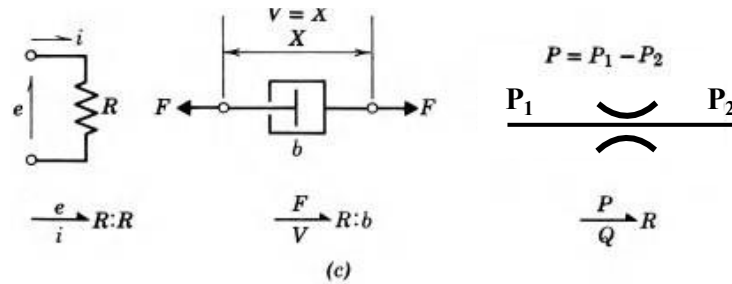


Figure A.2: resistance in different domains [K2012]

Capacitance or compliance relates effort to generalized displacement and it is an ideal energy storage.

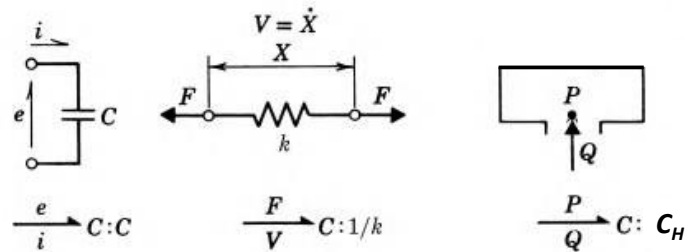


Figure A.3: capacitance in different domains [K2012]

Inductance relates flow to generalized momentum. As the capacitance, can store energy.

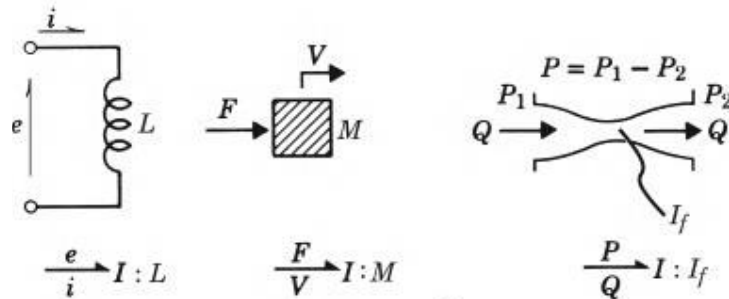


Figure A.4: inductance in different domains [K2012]

**Two ports components** are divided in transformers and gyrators. The transformer applies a transformation modulus  $m$  to the power variables, as shown in the following equations:

$$e_1 = m \cdot e_2, \quad m \cdot f_1 = f_2 \quad (\text{A.3})$$

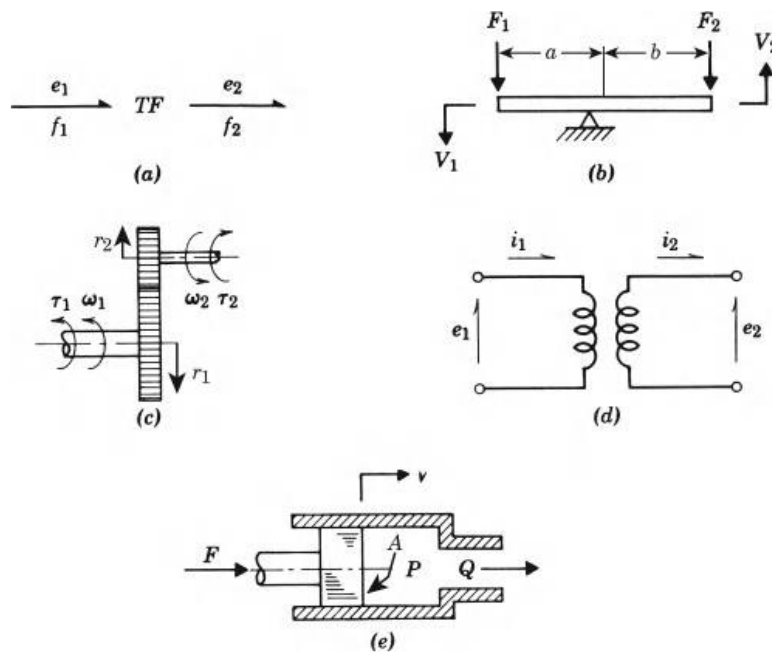


Figure A.5: transformers in different domains [K2012]

The gyrator correlates the input effort with the output flow and the other way around, applying the gyrator modulus  $r$ , as shown in the following equations:

$$e_1 = r \cdot f_2, \quad r \cdot f_1 = e_2 \quad (\text{A.4})$$

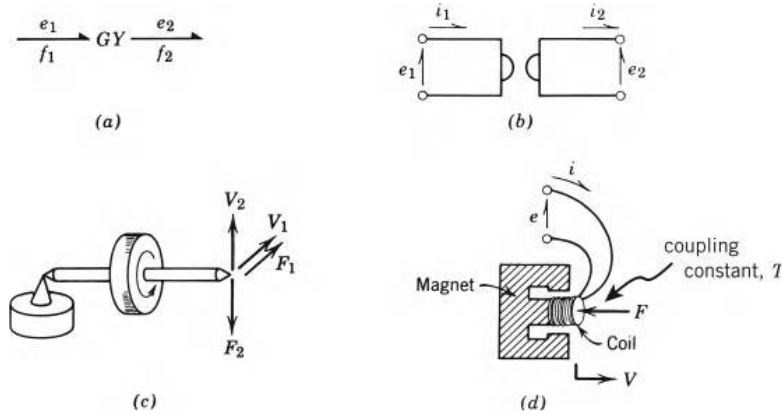


Figure A.6: gyrators in different domains [K2012]

Multiport elements are junction components, divided into 0 and 1 nodes. A 0 node is a common effort junction, the sum of flows in its ports is consequently null (can be demonstrated using the energy conservation principle). A 1 node is a common effort junction, for the same reason as node 0, the sum of efforts in its ports is null. The following table explains the physical principles behind them, for every domain [K2012].

Electrical circuits:	 —0—,	represents Kirchhoff's current law for a node where three conductors join
	 —1—,	represents Kirchhoff's voltage law written along a loop in which a current flows and experiences three voltage drops
Mechanical systems:	 —0—,	represents geometric compatibility for a situation involving a single force and three velocities that algebraically sum to zero
	 —1—,	represents dynamic equilibrium of forces associated with a single velocity—when an inertia element is involved, the junction enforces Newton's law for the mass element
Hydraulic systems:	 —0—,	represents the conservation of volume flow rate at a point where three pipes join
	 —1—,	represents the requirement that the sum of pressure drops around a circuit involving a single flow must sum algebraically to zero